Chapter 8

Raman Imaging of Lignocellulosic Feedstock

Notburga Gierlinger, Tobias Keplinger,
Michael Harrington and Manfred Schwanninger

Additional information is available at the end of the chapter

http://dx.doi.org/10.5772/50878

1. Introduction

The main structural plant cell wall polymers - cellulose, hemicelluloses, and lignin - rank amongst the most abundant biopolymers in Earth's carbon cycle. These three polymers form the lignocellulose complex and constitute the bulk of the cell wall with 40-50%, 10-40% and 5-30% of biomass by weight, respectively [1, 2]. Its highly ordered structure of cellulose microfibril aggregates, embedded in a matrix of hemicelluloses and lignin, provides the basis for its mechanical strength [3] and for the resistance to microbial attack [4], to which also low molecular mass extractives contribute [5]. Lignified cell walls are therefore a remarkably durable material. In nature, only higher fungi have developed biochemical systems to degrade the lignocellulose complex and perform the conversion and mineralisation of wood to carbon dioxide and water. Extensive reviews on decay pattern, chemistry and biochemistry of microbial wood degradation are available [4, 6, 7]. The natural processes occurring during fungal wood degradation may be utilised for industrial purposes and have a great potential for cellulose-producing and wood-processing industries as well as for high value-added conversion of lignocellulosic waste materials in *Biorefineries*. Particularly the molecular mechanisms of selective white-rot fungi offer a series of applications in the field of biotechnology of renewable resources [8].

Non-food biomass crops such as switchgrass (*Panicum virgntum* L.), *Miscanthus* x *giganteus,* and short-rotation coppice poplar and eucalyptus (*Populus* spp. and *Eucalyptus* spp.) [9] and willow (*Salix* spp.) offer a sustainable source of energy and platform for chemicals [10]. The absolute and relative contents of the cell wall components have a great influence on biomass quality i.e. its suitability for conversion to heat, power and chemical products. Biomass can be utilised by a number of thermochemical conversion routes (thermochemically, gasification, torrefication, flash pyrolysis) with differing feedstock demands and therefore measures of feed-stock quality are often quite specific [11, 12]. In contrast to the thermochemical processes where all plant cell wall polymers are converted to gases, the hydrolysis applications aim to convert carbohydrates into fermentable sugars. The

recalcitrance to saccharification is a major limitation for conversion of lignocellulosic biomass to ethanol, which is mainly due to the lignin [13] content and composition [14]. Lignin synthesis has extensively been investigated using lignin model compounds [15-17] and lignin from plants [18-22] and has been reviewed several times [23-25] including lignin structure [26] and wood formation in general [27, 28]. The lignin content in natural *Populus* variants affects sugar release [29] and how lignin composition, structure, and cross-linking affect degradability has been reviewed for cell wall model studies [30]. High lignin contents in the feedstock necessitate harsh chemical and heat pre-treatments prior to enzymatic saccharification [11]. This increases energy inputs and often damages the polysaccharide components of the cell wall giving rise to inhibitory products [31, 32]. Therefore considerable pressure arises to optimise feedstock composition. The most feasible way to achieve this is by breeding improvement [11, 33], although agronomic practice may also influence composition [34] as well as genotypic and environmentally derived variation in the cell wall composition [35]. The characterization of different lignification genes has stimulated research programmes aimed at modifying the lignin profiles of plants through genetic engineering. The first transgenic plants with a modification of lignin composition and lignin content have been obtained in 1995 [36]. Since this time a focus on genetic engineering of lignin content and composition can be observed [37-40]. The effect of downregulation of lignin biosynthetic enzymes on wood anatomy [41] and its biomechanics [42] has been investigated [43]. In stems of transgenic alfalfa lines recalcitrance to both acid pre-treatment and enzymatic digestion was found to be directly proportional to lignin content [44]. Some transgenics yield nearly twice as much sugar from cell walls as wild-type plants. Lignin modification could bypass the need for acid pre-treatment and thereby facilitate bioprocess consolidation [45].

Both, breeding of lignocellulosic biomass and the production of transgenic plants, places huge demands on the analyst in terms of methods that can cope with the differences in polymer composition and linkages between them and large sample numbers. Wet-laboratory methods are destructive and time demanding and do not allow handling large sample numbers. Nuclear magnetic resonance (NMR) spectroscopy [46-49], analytical pyrolysis [50, 51], thioacidolysis [52], and thermogravimetry [53, 54] allow to get information about the composition and linkages between the wood polymers, and ultra-violet (UV) microscopy allows to follow the distribution of e.g. lignin within the cell wall [55, 56]. The requirements on a well suited method are: 1) fast and cheap to allow high-throughput screening 2) non-destructive to probe the native cell wall 3) to be able to analyse the content of each component (cellulose, hemicellulose, lignin) 4) to analyse their distribution within the plant tissues down to the cell wall level and 5) linkages as well as the interdependencies within and between the wood components. Vibrational spectroscopic methods such as infrared [57] and Raman [58] spectroscopy have shown potential to fulfil these requirements and can contribute to understand the actual lignocellulosic substrate and what kind of chemical and microstructural alterations take place during breeding, genetic engineering, decay or processing.

Near infrared (NIR) spectroscopy, that enables analyses of high number of samples on a day basis, was used for the prediction of the content of wood components and mechanical properties [59, 60] and the assignment of bands in the near infrared region have been

reviewed recently [61]. Moreover it was shown that NIR spectroscopy can be used for the examination of the biodegradation of spruce wood by the white-rot fungi *Ceriporiopsis subvermispora* and that it is sensitive enough to differentiate between three applied strains [62]. NIR spectroscopy, which is often used in combination with multivariate data analysis, allows following the degradation of wood polymers [63-65]. Furthermore changes in interdependencies such as hydrogen bonding [66], and the accessibility of alcoholic and phenolic hydroxyl (O-H) groups to heavy water in non-degraded and brown-rot degraded spruce wood (*Piceas abies* L. Karst.) have been examined [67].

Mid infrared (MIR) spectroscopy allows similar investigations [68] as NIR spectroscopy with the advantage of better separated bands in the fingerprint region and the possibility of revealing the orientation of polymers and their interactions, which is of utmost importance in lignocellulose feedstock utilization. Dynamic Fourier transform infrared (FT-IR) spectroscopy has been shown to be appropriate for studying interactions among wood polymers and their ultrastructural organization [69-72]. In spruce wood fibres a close cooperation between cellulose and glucomannan in the fibre wall was suggested, whereas xylan showed no mechanical interaction with cellulose [69]. In primary cell walls investigations indicated a strong interaction among lignin, protein, pectin, xyloglucan, and cellulose [73]. Furthermore the orientation of cell wall polymers can be elucidated by polarised FT-IR measurements. In spruce glucomannan and xylan appear to have a parallel orientation with regard to the orientation of cellulose and, in all probability, an almost parallel orientation with regard to the fibre axis [74]. The first evidence for lignin orientation within native wood cell walls was revealed by Raman microprobe studies [75] and later confirmed in the secondary wall of tracheids fibres of thermomechanical pulp by FT-IR [70]. Very recently H-2 NMR spectroscopy was used to quantify lignocellulose matrix orientation with the ability to separately investigate oriented and unoriented amorphous domains in intact natural plant tissue [76].

Mid-infrared spectrometers can like Raman spectrometers be coupled to a microscope to reveal spatial resolution on the micron-level. Polarised FT-IR microscopy confirmed the preferential alignment of lignin in the direction of the fiber axis within the cell wall, but no orientation was found for the lignin in the middle lamella [77]. In combination with a fluid cell FT-IR microscopy was used to monitor *in-situ* the enzymatic degradation of cellulose-treated cross-sections of poplar (*Populus nigra* × *P. deltoids*) wood [78]. The accessibility of cellulose within the lignified cell wall was found to be the main limiting factor, whereas the depletion of the enzyme due to lignin adsorption could be ruled out. The fast, selective hydrolysis of the crystalline cellulose in the G-layer, even at room temperature, might be explained by the gel-like structure and the highly porous surface. Young plantation grown hardwood trees with a high proportion of G-fibres thus represent an interesting resource for bioconversion to fermentable sugars in the process to bioethanol [78]. FT-IR microscopy has been used to identify and characterise cell wall mutants [79-81] and transgenic plants altered in cell wall biosynthetic genes [82]. The localisation and characterisation of incipient brown-rot [83] and simultaneous and selective white-rot decay [84] within spruce wood cell walls was possible using FT-IR imaging microscopy. FT-IR microscopes equipped with focal plane array detectors allow very rapid chemical mapping over large areas with a spatial resolution

limited by the wavelength of the infrared radiation to 10 - 5 μm. Thus single plant cells, which range generally between 10 - 50 μm in diameter, are resolved, but cellular components and cell wall layers may be substantially smaller and therefore below the limit of resolution. To overcome this limitation and get resolution on the cell wall layer level or for *in-situ* measurements of wet samples Raman microscopy imaging with a spatial resolution below 0.5 μm became the method of choice.

2. Basic principles, instrumentation, techniques and data analysis

2.1. Basic principles and Instrumentation

Raman and infrared spectroscopy monitor molecular vibrations, but are based on different principles. Raman spectroscopy involves inelastic scattering with a photon from a laser light source while IR spectroscopy involves photon absorption, with the molecule excited to a higher vibrational energy level. Thus, unlike infrared absorption, Raman scattering does not require matching of the incident radiation to the energy difference between the ground and excited states. In Raman scattering, the light interacts with the molecule and distorts (polarizes) the cloud of electrons round the nuclei to form a short-lived 'virtual state' before re-radiation. If only electron cloud distortion is involved in scattering, the photons will be scattered with very small frequency changes, as the electron mass is comparatively low. This elastic scattering process is the dominant process and called Rayleigh scattering. However, if nuclear motion is involved energy will be transferred either from the incident photon to the molecule (Stokes) or from the molecule to the scattered photon (Anti-Stokes) [85]. In the Raman scattering process the energy of the scattered photon is different from that of the incident photon (Raman-shift). Raman scattering therefore depends on changes in the polarizability due to molecular vibrations. On contrast IR absorption is based on changes in the dipole moments. Raman and IR spectroscopy thus provide "complementary" information about the molecular vibrations of a given sample. While water gives a strong absorption band in the IR (dipole), only weak Raman scattering is observed making this technique very suitable for *in-situ* studies of biological material.

The Raman scattering process is inherently a very weak process and only one of every 10^6–10^8 photons is affected. It was experimentally the first time proven in 1928 and the first Raman spectra had to be recorded with very long acquisition times [86, 87]. The development of lasers in the 60's brought the method a big step forward as the Raman signal is proportional to the excitation power. Today the excitation laser power has to be adjusted well below the point where absorption leads to thermal decomposition of the sample, especially when biological materials are investigated. Furthermore, the Raman scattering intensity is proportional to υ^4, where υ is the frequency of the exciting laser radiation [85]. Excitation at 400 nm (=$7.5*10^{-14}$ Hz) therefore leads to about 16 times higher Raman signal than excitation at 800 nm (=$3.75*10^{-14}$ Hz). But when measuring biological materials several components absorb the light in the lower wavelength range and therefore sample fluorescence can become problematic and swamp the Raman signal or even thermal sample decomposition may occur. Moving from the visible to the near-infrared (NIR) range,

fluorescence virtually disappears as electronic absorption bands are unlikely. The use of Nd:YAG (neodymium-doped yttrium aluminum garnet) laser radiation at 1064 nm coupled with interferometers (involving Fourier transformations) led to so-called near infrared Fourier Transform (NIR-FT) Raman spectrometers [88]. Laser with wavelength in the visible range (e.g. Ar^+, He–Ne, Kr^+, doubled Nd:YAG lasers) are usually coupled with a dispersive spectrometer and a charge coupled device detector (CCD) for detection (Figure 1). These classical dispersive multichannel Raman spectrometers are nowadays often used in confocal microscope configurations with the advantage of superior rejection of fluorescence and depth resolution due to the pinhole [89].

For Raman microscopy, and especially for the imaging approach, the throughput of the radiation in the system has to be optimised in every part to acquire spectra fast and of high quality (high signal to noise (S/N) ratio). If a single spectrum is acquired, it is usually not important whether the necessary integration time is 0.1 s or 10 s. However this becomes an issue in scanning (mapping) experiments (imaging), when it becomes 15 min or 25 h. Therefore perfect coupling of the laser radiation into the microscope and out to the spectrometer is important as well as high throughput in the spectrometer and high detection efficiency of the CCD camera [90]. Optical fibres serve as ideal light pipes for connecting the elements and as a pinhole for the outgoing scattered radiation (Figure 1). Furthermore using a spectrometer optimized for the used wavelength range ("blazed" gratings) can increase the throughput as well as CCD cameras most sensitive for the chosen excitation wavelength [90, 91].

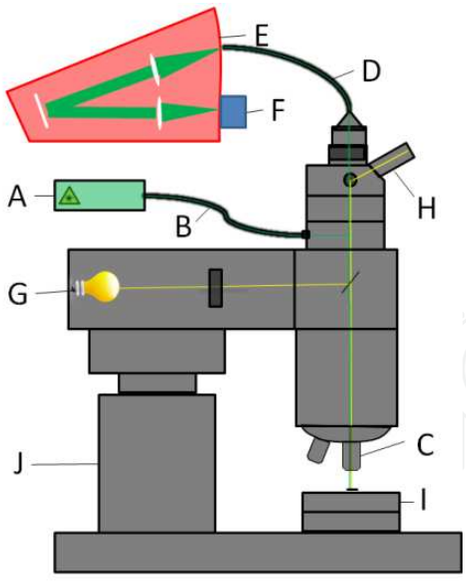

Figure 1. Typical set up of a confocal Raman microscope: The excitation laser (A) is focused via an optical fibre (B) and a microscope objective (C) onto the sample. The backscattered light is coupled out into a fibre (D), which acts as a pinhole. After passing the spectrometer (E) the signal is detected by a CCD camera (F). For visual inspection of the sample usually a white light source (G) and a camera (H) for picture capturing is available. For mapping/scanning the system is equipped with a piezo-driven X-Y- stage (I) and a Z-stage (J).

2.2. Resonance Raman spectroscopy, Surface Enhanced Raman Spectroscopy (SERS) and Coherent Anti-Stokes Scattering (CARS)

When a powerful beam of radiation is used some atoms and molecules of a sample absorb radiation at particular wavelengths and the e.g. coloured molecules become excited. Subsequently radiation of longer wavelength - termed fluorescence - is emitted. This fluorescence can be strong (intensive) and prevent the detection of the (weak) Raman signal [85]. But when the frequency of the laser beam is close to the frequency of an electronic transition, scattering enhancements of up to 10^6 have been observed. In this resonance condition (Resonance Raman spectroscopy) the method becomes much more sensitive and since only the chromophore gives the more efficient scattering, it will also be selective for the part of the molecule involving the chromophore [85, 92, 93]. Furthermore fluorescence suppression can be achieved by using Kerr gating [93-95].

Another way of enhancing Raman intensity is to disperse the sample on metallic surfaces (either roughened wafers or colloidal solutions). The photon – plasmon interaction results in a huge signal enhancement and the technique, called surface-enhanced Raman spectroscopy (SERS), has progressed from studies of model systems on roughened electrodes to highly sophisticated studies, such as single molecule spectroscopy and molecular imaging [96-98]. The advantage is to enhance the Raman signal and besides the SERS effect leads to fluorescence quenching [99].

Another way of circumventing fluorescence is coherent anti-Stokes Raman scattering (CARS). This technique allows vibrational imaging with high sensitivity, high spectral resolution and three-dimensional sectioning capabilities. It is a nonlinear diagnostic technique that relies on inducing Raman coherence in the target molecule using two lasers, probed by a third laser which generates a coherent signal in the phase-matching direction at a blue-shifted frequency. Because of this nonlinear intensity dependence the photo-damage of the sample is reduced and the efficient background rejection improves the quality of the spectra [100]. CARS microscopy has already been used for imaging a number of delicate biological samples and processes, e.g. imaging of C–H stretching vibration present in the lipid bilayer of the cell membranes [101-103]. Two other Raman imaging techniques with great potential have evolved recently: Stimulated Raman scattering spectroscopy and Ultrafast Raman loss spectroscopy [104-107].

2.3. Spatial resolution and Tip-Enhanced Raman Spectroscopy (TERS)

The spatial resolution in Confocal Raman microscopy is limited by the diffraction of radiation and defined by the distance between the central maximum and the first minimum of the diffraction pattern, which is given by $r = 0.61\ \lambda / NA$ (λ = wavelength of the radiation, NA = numerical aperture of the objective) [108]. If high spatial resolution is sought-after, a laser in the visible range (e.g. 532 nm versus 1085 nm) and a microscope objective with a high numerical aperture (NA>1) have to be chosen. NA is defined by the refractive index of the medium (n) in which the optics are immersed (e.g. 1.0 for air and up to 1.56 for oils) and the half-angle of the maximum cone of radiation that enters or exits the condenser or

objective (θ) (NA = n.sinθ). Two objects are completely resolved if they are separated by 2r and barely if they are separated by r (Rayleigh criterion of resolution) [108]. Therefore, the highest spatial resolution can be achieved with oil immersion objectives with high NA. Also if depth resolution is important, immersion objectives (oil, water) give better results [109]. Generally the axial resolution is around twice the lateral resolution [110].

Tip-enhanced Raman spectroscopy (TERS), which is based on the surface plasmonic enhancement and confinement of light near a metallic nanostructure, can overcome the so-called diffraction limit and produce optical images far beyond. It has been demonstrated that a spatial resolution as high as 4 nm could be achieved [111]. Consequently, nucleobases, proteins, lipids, and carbohydrates can be identified and localized in a single measurement. This has been shown in the last few years for different biological samples ranging from single DNA strand investigations to cell membrane studies [111-113].

2.4. Raman approaches for imaging

The main methods for Raman imaging are scanning (mapping) methods (Point-by-Point and Line scanning) and Wide-field source illumination approaches [114-117].

In Point-by-Point scanning the sample is scanned with a laser beam using X, Y, Z scanning stages. At each position of the raster a Raman spectrum is acquired and out of these spectra an image generated. The laser and the scattered light are often focused through so-called pinholes in order to know the exact position of the excitation and the collection volumes from the samples. The limiting factor of the Point-by-Point scanning approach is the fact that quite long measuring times are necessary because the duration is proportional to the number of pixels. Nevertheless the main advantage is that the whole Raman spectrum is acquired at each point and available for detailed analysis [114].

In the Line scanning approach the laser is elongated (1 dimension) to form a line with the help of a moving mirror or cylindrical optic devices. As a result the sample is illuminated with a laser line, which is parallel oriented to an entrance slit of a dispersive spectrograph. Scanning of the sample is still required, but only in the direction perpendicular to the laser line. This leads to a reduced experiment time [114]. It is the most efficient method if the spectral information from areas with perimeters of typically a few millimetre is required [116].

In Wide-field Raman imaging the whole sample field is illuminated with laser light. The experimental time depend primarily on the number of spectral channels or wavenumber positions at which an entire image is recorded [116]. There are numerous Wide-field Raman imaging approaches, such as liquid crystal tuneable filters (LCTFS) or the Fibre Array Spectral Translator (FAST). In FAST the received Raman light from a globally illuminated sample field is focused on a 2-dimensional array of optical fibres, which is followed/reduced to a one dimensional array on the distal end. This end is imaged through a dispersive spectrometer with a CCD detector. This method makes it possible to reduce two spatial dimensions data to a

single dimension, which is afterwards dispersed fibre by fibre onto the CCD camera [114]. To characterize a sample´s chemical heterogeneity often only a few global Raman images need to be recorded at well-defined wavenumber positions, which are known either a priori or from spectral analysis of data obtained in point or line scanning [116].

As a non-destructive technique in general minimal or no sample preparation is necessary. Nevertheless to refer intensity changes in imaging approaches directly to changes in content or composition the same Raman scattering volume has to be probed at any position and this requires a flat surface. Otherwise a reference band for normalisation or the use of band ratios becomes necessary. Depending on the biological material to be probed microcutting or polishing might be the method of choice to achieve such a flat surface, with or without embedding [118, 119].

2.5. Processing of Raman spectra and image generation

To take the advantage of the scanning (mapping) method to have a molecular fingerprint (whole spectrum) at every pixel sophisticated data analysis has to be applied. Typically in each scanning experiment thousands of spectra are acquired and extracting the relevant information needs usually pre-processing of the spectra (e.g. cosmic ray removal, background subtraction, smoothing…) followed by univariate or multivariate data analysis methods to generate images.

2.5.1. Spectra pre-processing

Raman instruments utilizing CCD detectors suffer from occasional spikes caused by cosmic rays. Cosmic rays are high energy particles from outer space which interact with atoms and molecules in the earth´s atmosphere and may generate a false signal in the shape of a very sharp peak in the spectrum. Various mathematical methods can be used to filter the cosmic rays from the spectra [120-122]. As the spikes are usually quite high and may overlay with bands of interest they have to be removed to avoid influences on the final results.

Smoothing algorithms are used to reduce noise in the recorded Raman spectra. They rely on the fact that spectral data are assumed to vary somewhat gradually when going from one spectral data point to the next, whereas associated noise typically changes very quickly. Different algorithms can be chosen (e.g. Savitzky-Golay [123], wavelet transformation [124], maximum entropy filter [122]) and especially before multivariate data analysis smoothing might become necessary.

Baseline correction and background subtraction can be performed based on linear models or on more complex mathematical functions. For removing background coming from the measured material (fluorescence) or signal from the substrate different methods have been developed that are capable of handling irregularly shaped baselines [125-128]. Baseline correction of Raman spectra is especially important prior to multivariate methods and different solutions to improve baseline correction methods have been developed [125, 129, 130].

Additional pre-treatments can be carried out to enhance certain properties of the image data set. The choice depends on the spectral structure and the goal of the data analysis. Derivatives can be carried out to stress subtle differences in spectral features among spectra. For pixel classification purposes, when the focus is on comparing the shapes of the pixel spectra independently from their global intensity, spectra normalization represents a useful option [126].

2.5.2. Univariate and multivariate image generation

In univariate data analysis each spectrum determines one value of the corresponding pixel in the image. The value of each pixel is determined by simple filters or by fitting procedures [122]. The most important of the simple filters is the integrated intensity (sum) filter evaluating the integrated intensity of various specific peaks found in the spectra of the image scan. The amount and scattering strength of a certain band attributed to a specific component is displayed and gives information on its spatial distribution. Filters can also plot changes in peak width, which can give a measure of crystallinity and structural orientation or changes in peak position (i.e., centre of mass position) as a measure for the strain within the material [131].

Many different multivariate methods exist and are described in detail elsewhere [126, 132-136]. Here only the very basics of the most commonly used ones, principal component analysis (PCA) and cluster analysis, are introduced.

PCA is the underlying method for many other multivariate methods since it is very effective for data reduction. It may be used to reduce the data set to 5–15 principal components (PC) and the residual error. Principal components are new, uncorrelated, and approximately normally distributed variables that provide faithful representations of the image, which can be used later as input information for exploration, segmentation, classification and other purposes. Compression by using principal components keeps all the relevant (image) information and, at the same time, allows understanding the relationship among the variables used to build the model by analysing the internal correlation structures provided by the loadings [132].

Cluster analysis applied to Raman images is essentially the sorting of the tens of thousands of spectra in a data set according to their similarities [122]. There are various ways of clustering, e.g. distance calculation (Euclidean, Manhattan), hierarchical cluster analysis, K-means Cluster Analysis, Fuzzy Clustering and each has its advantages and disadvantages [136].

In section 4 and 5 exemplary results for univariate analysis (band integration) and cluster analysis are shown.

3. Raman spectra of plant cell walls: What information can we gain?

Plant cell walls are nanocomposites based on cellulose microfibrils embedded in different matrix polymers (hemicelluloses, pectin and lignin) [137]. Besides water plays an essential

role in the native plant cell walls and as water has relatively low polarizabilities weak Raman intensities are observed. Consequently, water saturated samples can be measured without problems. Raman investigations of cellulosic feedstock started in the 80s with the acquisition of spectra of cellulose fibres and wood [138-140].

3.1. Cellulose microfibrils: The structural elements of the cell wall

The cellulose microfibrils give a Raman signature comprising about 15 different significant bands (Figure 2, ramie fibre: almost pure cellulose). If these microfibrils are aligned with a preferred orientation, the Raman intensity of the cellulose bands depends on the angle between the orientation of the cellulose microfibrils and the laser polarisation direction [138]. The investigated Ramie fibres have almost perfect alignment of the cellulose microfibril parallel to the fibre axis and high crystallinity (X-ray results, not shown). Changing the laser polarization from parallel with respect to the fibre axis (0°) to perpendicular to the fibre (90°) results in severe changes of the Raman intensity of almost all characteristic bands (Figure 2) except the two bands at 1377 and 437 cm^{-1}. The bands at 1457 cm^{-1} (HCH and HOC bending), 517 cm^{-1}, 499 cm^{-1} and 378 cm^{-1} (heavy atom stretching) show higher intensity in 90° arrangement and thus a more perpendicular alignment of these groups (Table 1). The β–(1→4)-glycosidic linkages in cellulose molecules, the methine groups of the glucopyranose rings and the methylene groups of the glucopyranose side are heavily orientation-dependent and reflect the cellulose molecule orientation along the fibre axis.

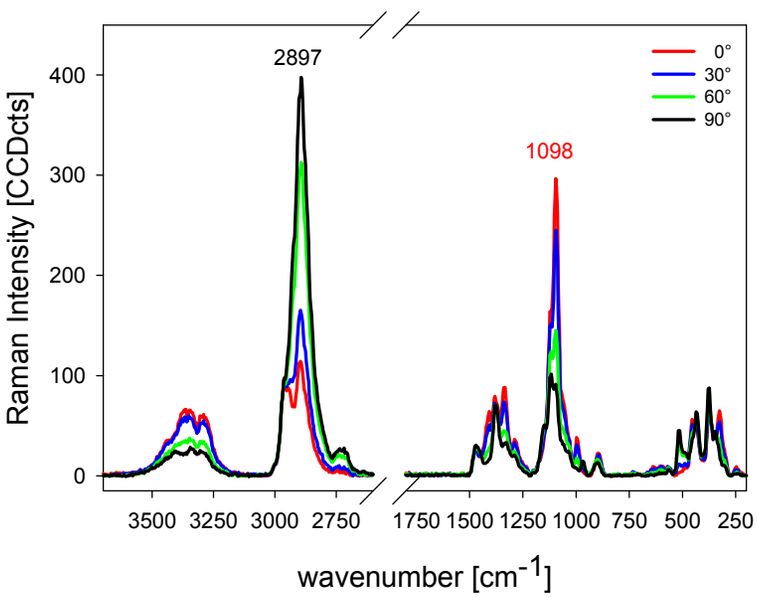

Figure 2. Raman spectra (532 nm excitation, 0.25 s integration time, 10 accumulations, baseline corrected) acquired from a Ramie fibre (>95% cellulose, high crystallinity, microfibrils aligned parallel to the fibre axis) with changing the polarization direction of the incident laser from 0° (parallel to the fibre axis and cellulose fibrils) to 90° (perpendicular to the fibre axis).

Band [cm^{-1}]	Assignment	Molecular orientation *
330	δ (CCC) ring	∥ s
380	δ (CCC) ring	⫩ m
436	Γ (COC) def	⫩ m
497	ν (COC) glycosidic	⫩ m
520	δ (COC) glycosidic	⫩ s
902	υ (COC) in plane, sym	∥m
970	ϱ (CH_2)	⫩ m
998	ϱ (CH_2)	∥ s
1098	υ (COC) glycosidic, asym	∥ s
1121	υ (COC) glycosidic, sym	⫩ m
1340	ω (CH_2)	∥s
1380	δ (CH_2)	◦
1472	δ (CH_2); δ (COH);	⫩ m
2897	υ (CH)	⫩ s
3200-3500	υ (OH)	∥s

Table 1. Position and assignment [138, 141] of the cellulose bands (Ramie fibre, Figure 2) and their preferred molecular orientation parallel (II) or perpendicular (⫩) to the fibre axis direction (=laser polarisation direction). The sensitivity of the bands to intensity changes due to orientation is referred to as no changes (◦) and strong (s) or medium (m). (def: deformation, sym: symmetric, asym: antisymmetric)

Because of the orientation-dependence of the cellulose band intensities, the fibre direction (plant axis) and the laser polarization have to be adjusted in a known and defined way in every plant cell wall Raman experiment. As the intensity of multiple bands change in a characteristic way (up and down, Figure 2), it is possible to distinguish between intensity changes due to alterations in fibre orientation from those resulting from different cellulose content (all bands increase or decrease). To eliminate intensity changes due to different focal plane during rotating the polarizer or drift of the scan stage band height ratios or band area ratios can be calculated for a more detailed analysis (Figure 3A). These ratios also allow the comparison of Raman measurements with different integration times and thus intensity. The ratios (2897/1095, 378/1095 and 1377/1095) reveal a clear dependency of the cellulose band intensities and the angle of the incident laser polarization. The strong relationship can be described by a cosine function and a quadratic regression (R^2>0.99). Based on the band height ratios (Figure 3B) or partial least square regression models the angle of the cellulose molecule with respect to the laser polarisation direction and consequently the microfibril angle can be calculated [142]. Noteworthy, changes in fibre orientation often correspond to alterations in cellulose crystallinity. The effect of changes in crystallinity on the shape of the cellulose Raman bands was also investigated in detail: amorphous cellulose results in a significant decline in band heights accompanied by band broadening [143].

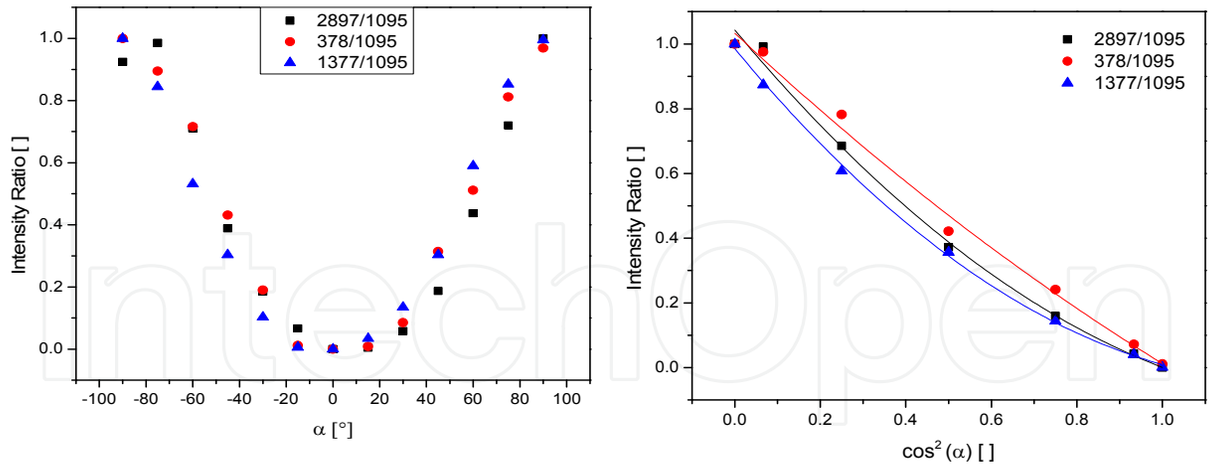

Figure 3. A-B. Relationship between the intensity ratios of cellulose bands and the angle of laser polarization α (A, B: accounting for a cosine function with a quadratic regression)

3.2. Carbohydrate matrix polymers: Hemicelluloses and pectin

Hemicelluloses and cellulose have similar functional groups and chemical bonds and therefore the Raman contributions are overlapping. Due to the more amorphous nature of hemicelluloses the Raman signal intensity is less and the bands are usually broader [144]. According to Himmelsbach et al. [145] the weak bands between 870–800 and 515–475 cm^{-1} offer the potential to distinguish between cellulose and xylan in flax fibres. In *Miscanthus* a characteristic band at 478 cm^{-1}, assigned to HCC and HCO bending at C6 of hemicelluloses was used to present the hemicellulose distribution [146]. Nevertheless within wood and pulp samples the bands typical for glucomannan and xylan were hardly detected [144]. Distinguishing and probing the hemicelluloses in cell walls with the Raman imaging approach is therefore not that straightforward and needs sometimes more sophisticated data analysis tools to resolve the overlapping and less intense characteristic bands.

While cellulose and hemicelluloses have β-glycosidic bonds, pectins are composed of α-glycosidic linkages. In the Raman spectrum the region between 860-825 cm^{-1} corresponds to equatorial anomeric H (α-anomers and α-glycosides), whereas the band at about 900–880 cm^{-1} corresponds to axial anomeric H (β-anomers and β-glycosides) [147]. The sharp Raman band between 860 and 854 cm^{-1} is characteristic for pectin and shows no overlap with the other plant cell wall polymers and can therefore be used as a marker band in the imaging approach [148, 149]. Furthermore the exact position of this band is sensitive to the state of uronic carboxyls and to *O*-acetylation thus providing insight into pectin structure; decreasing with methylation (min. 850 cm^{-1}) and increasing with acetylation (max. 862 cm^{-1}) [150].

3.3. The aromatic lignin polymer: Fluorescence and diversity

The structure of lignin is comprised of a variety of different types of covalent bonds derived from oxidative coupling of three different types of phenolic precursor units, p-coumaryl,

coniferyl, and sinapyl alcohols [151, 152]. The structural organisation of lignin is a subject of much debate, both in terms of chemical structure (H (p-hydroxyphenyl), G (guaiacyl) and S (syringyl) units/monomers and the bondings) and in terms of the degree to which lignin is ordered within its cell wall environment. Beside NMR and IR spectroscopy also Raman microscopy has shown high potential for non-invasive investigation of *in-situ* cell wall lignin structure during the last years e.g. [153, 154].

Laser-induced autofluorescence from lignin can be the major hindrance to acquire reasonably good Raman spectra because the fluorescence intensity can be several orders of magnitude larger than the Raman scattering intensity. Traditionally, two sampling procedures were used to effectively reduce the autofluorescence: water immersion technique (usable for woody tissues) [140] and oxygen flushing technique [155]. Fluorescence problems can be reduced by choosing the near-IR Fourier transform (NIR-FT) Raman technique, using a NIR laser source with the photon energy well below troublesome low energy electronic transitions of lignin. Good quality spectra, relatively free of fluorescence interference, have been acquired from various lignin-containing materials [156-161]. Today, also more sophisticated spectroscopic methods can overcome this problem. UV resonance Raman spectroscopy exploits the combined benefit of the resonantly enhanced Raman signal and the usually relatively much longer wavelengths of fluorescence emission compared to Raman photons [153, 162-164]. By Kerr-gated Raman spectroscopy the different time-domain characteristics of fluorescence and Raman emission allow the detector only to see a narrow time-domain window centred on the excitation laser pulse [93, 164]. Also CARS gives spectra free of background from one-photon-excited fluorescence and has been used to study lignin modification in alfalfa [165]. All the significant instrumental developments opened up new fields for investigating lignified samples.

Improvements in Confocal Raman mapping/imaging approaches have provided insights into lignin distribution on the microscale. Due to the high spatial resolution it is possible to acquire spectra comprising only the chemistry of the cell corner, which is in lignocellulosics dominated by lignin contribution (Figure 4). The imaging approach requires short integration times (e.g. 0.1-0.4 s) and therefore not all lignin bands are resolved and the spectra are dominated by the strong band around 1600 cm^{-1} (Figure 4A), which is assigned to aryl stretching vibrations [166]. As this band has no overlap with the carbohydrate bands it can be used as a marker to image lignin distribution on the micron level [167, 168]. Depending on laser excitation and lignin structure, more or less background or resonance enhancement is observed. Due to the different chemical structure of softwood and hardwood lignin particular laser excitation (e.g. 532 nm) results in a higher fluorescence background and stronger 1607 cm^{-1} band intensity in spruce than in poplar. In softwood species, the most abundant precursor is coniferyl alcohol, which leads to an aromatic substitution by one methoxyl group, known as a guaiacyl structure (G lignin). In hardwood additionally sinapyl alcohol leads to syringyl structures (S lignin) with two methoxyl groups attached to the aromatic ring. Additionally, during the formation of the middle lamella

p-coumaryl alcohol precursors are present and p-hydroxphenyl lignin without methoxyl groups is formed. The differences in lignin structure in the cell corner of spruce and poplar are reflected by the different intensity and band shape in the region at about 1600 cm^{-1} as well as in the other bands (Figure 4A). Contribution from coniferaldehyde units is expected at 1623 and 1660 cm^{-1}, whereas coniferyl alcohol contributes at 1654 cm^{-1} as well as other chromophores [169]. Using these bands the amount of coniferyl alcohol and aldehyde groups compared to the total amount of lignin was imaged in pine and spruce wood samples [170]. For the S units the intense band at 1328 cm^{-1} is characteristic, while in spruce the band is found at 1334 cm^{-1} [144] and accompanied by bands (shoulders) below and above (Figure 4A, Table 2). The relatively intensive band at about 1150 cm^{-1} in poplar wood was tentatively assigned (Table 2). On the contrary, in spruce the band at 1139 cm^{-1} is stronger (Figure 4A).

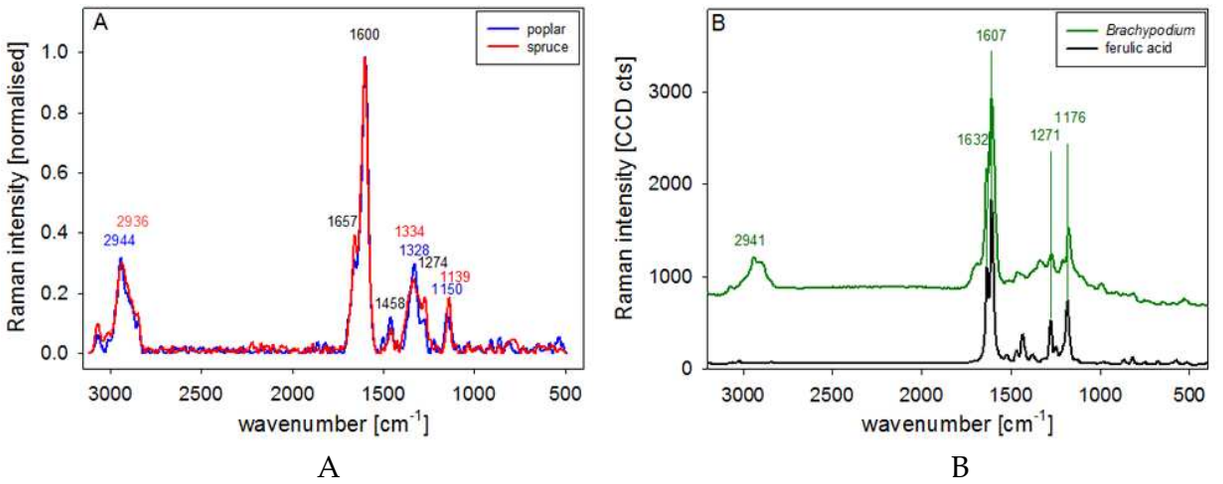

Figure 4. A-B. Raman spectra (532 nm excitation, 0.1-0.4 s integration time) acquired from the cell corner of wood (poplar and spruce, A) and *Brachypodium* (B), reflecting the different lignin structures in softwood, hardwood and grasses. Additionally a reference spectrum of ferulic acid is plotted (B, black line)

Grasses have Type II cell walls, which in addition to other cell wall polymers, typically contain arabinoxylans and phenolics [171-173]. Noteworthy, grass xylans play an important role in the cell wall by helping to facilitate the assembly of cellulose microfibrils or/and the cross-linking of lignin to polysaccharides with the aid of hydroxycinnamic acids [174]. When compared to dicots, a high amount of hydroxycinnamic acids (ferulic and p-coumaric acid) is characteristic for grass cell walls. Therefore the cell corner spectrum of *Brachypodium* (Figure 4B) differs remarkably from the wood spectra (Figure 4A). The very strong aryl stretching vibration at 1607 cm^{-1} is a clear doublet with a second band at 1632 cm^{-1}, accompanied by a weaker band at 1701 cm^{-1}. This doublet peak as well as the bands at 1176 cm^{-1} and 1276 cm^{-1} are typical for ferulic acid [175, 176] (Figure 4B). So the cell corner spectra of *Brachypodium* clearly reflect contributions from ferulic acid. Similar bands have been found in corn stover, although not recognized to be due to ferulic acid [177].

Spruce	Poplar	*Brachypodium*	Assignment [Reference]
Wavenumber [cm^{-1}]			
2936	2944	2941	antisymmetric C-H str. in OCH_3 (SW) [178] and (HW) [179]; symmetric C-H str. in CH_3 in FA [180]
1657	1657		ring-conjugated C=C str. of coniferyl alcohol plus C=O str. of coniferaldehyde [178, 179]
		1632	str. of C=C from propenoic acid side chain of FA [180]
1599	1600	1607	symmetric aryl ring str. [144, 166-168]
1503	1498	1505	antisymmetric aryl ring str. [178], in FA
1458	1458		C-H_3 def. in O-CH_3 [179]; C-H_2 scissoring; guaiacyl ring vibration (SW) [178, 179] and to C-H_3 def. in O-CH_3 (HW) [166, 179]
1334	1328		aliphatic O-H bend. (SW) [144, 178], and S-lignin (HW) [177], possibly contribution from cellulose
1271	1274	1271	aryl-O str. of aryl-OH and aryl-O-CH_3; guaiacyl ring (with C=O group) mode (SW) [144, 178, 179], HW [177, 179]
		1176	aryl-H def. [180]
	1150		eventually O-CH_3 def. [166]; possibly contribution from carbohydrate [177]
1139			a mode of coniferaldehyde unit (SW) [178]; aromatic C-H in plane def. (guaiacyl type) [181]

Table 2. Position and assignment of lignin bands in spectra acquired from the cell corners of spruce, poplar, and *Brachypodium*; FA: ferulic acid; SW: softwood; HW: hardwood; str: stretching vibration; bend: bending vibration; def: deformation vibration

4. Raman imaging of wood: Revealing lignification on the micron level

In the future, wood will play a crucial role in carbon capture and is a fundamental feedstock for bio-based fuels, chemicals, materials, and power. Currently, the greatest processing challenge is to develop efficient deconstruction and separation technologies that enable the release of sugar and aromatic compounds 'locked in' the intricacy of wood cell wall macromolecular structures [182]. To tackle this challenge detailed knowledge on the molecular composition of the cell walls within the different cell wall tissues and layers is of importance and Raman microscopy may contribute to make progress. As a non-destructive method, characterisation of the native cell walls is possible as well as the *in-situ* monitoring of the deconstruction during different treatments.

By calculating the integral of the bands in the Raman spectra of plant cell walls the distribution of different molecular structures can be imaged on the micron-level [148, 149,

167, 183]. Figure 5A shows an example of imaging water uptake of cell walls in young poplar wood (*Populus nigra x Populus deltoids*) by plotting the integral of the OH stretching vibration. As the sample was water saturated, highest intensity (blue colour) is observed in the water filled lumen of the cells. The border to the cell wall is slightly visible as less blue, followed by remarkable high intensity of the inner cell wall layer. Clear distinct layers separating the cells are visualised black and thus less hydrated areas. Integrating the strong aromatic aryl stretching vibration gives the opposite picture (Figure 5B): high intensity (red colour) in the cell corner (CC) and compound middle lamella (CML) and the rest of the cell walls are displayed black as intensity is less than to be seen with this scaling. In contrast the inner layer (gelatinous (G-) layer) of the poplar tension wood can be visualised selectively by integrating the 1380 cm^{-1} cellulose band. This band is not sensitive to changes in cellulose orientation (Figure 2A). In lignified samples the band becomes a shoulder the more the adjacent lignin band rises and therefore only in cellulosic cell wall regions without (or very minor) lignin the band is clearly resolved and shows high intensity by integration. So the black regions of the images not necessarily represent non-cellulosic regions, but regions where cellulose is accompanied by higher lignin content. Based on the lignin and cellulose images three cell wall regions have been selected by using an intensity threshold (Figure 5D): 1) lignin intensity higher than 3000 cts (red), 2) lignin intensity between 1000 and 3000 cts (pink) and 3) cellulose intensity higher than 150 cts (green). The highest lignin content comprises the CC regions as well as part of the vessel walls (v) (Figure 5D, red). Medium lignin content displays the CML (and probably part of the S2 layer) as well as the ray cells (Figure 5D, pink) and the non-(or minor) lignified region is restricted to the inner cell wall (Figure 5D, green). For a detailed analysis of the cell wall regions, average spectra can be calculated from the defined cell wall regions of the sample (Figure 5E). For better comparison spectra have been baseline corrected and normalised to the aromatic lignin stretching vibrations. The spectra show that lignin is present in the green coloured cell wall region (G-layer) in minor amounts and the carbohydrate bands (C) are in relation much higher as well as the OH and CH stretching vibrations. Numerous OH-groups are present in the carbohydrates and show a contribution in the cellulose Raman spectra (Figure 2). But the height and form of the OH-bands in the G-layer are more comparable to spectra from the free water in the lumen and thus point to access of water uptake in this inner layer. In the medium lignified region (pink), similar cellulose bands are detected, but only one third of intensity compared to the inner layer. In the highly lignified region the lignin signature dominates (Figure 5E, red line). Yet carbohydrate bands are abundant, mainly because also the highly lignified vessel walls (v) are partly included in the average spectra calculation. Vessel spectra show higher amount of carbohydrates than spectra from CML (not shown). A zoom into the "lignin region" shows that not only the amount changes on the micron level, but also the lignin structure: a slight shift in band position of the aromatic stretching vibration is observed and the height of the shoulder at about 1657 cm^{-1} changes. As the sampled region is near the cambium and the higher shoulder points to the alcohol and aldehyde lignin precursors in the G-layer and S2, lignification process in these regions might be in progress. Interestingly also spectra derived from substances within the rays point to aromatic compounds. These deposits could be visualised selectively by integrating from

785-486 cm^{-1}. Detailed analysis of the spectra and band assignment will reveal the composition of these ray components. Several studies have shown that molecular structures, e.g. lignin structure are reflected in the Raman signature [154, 161, 170, 184, 185].

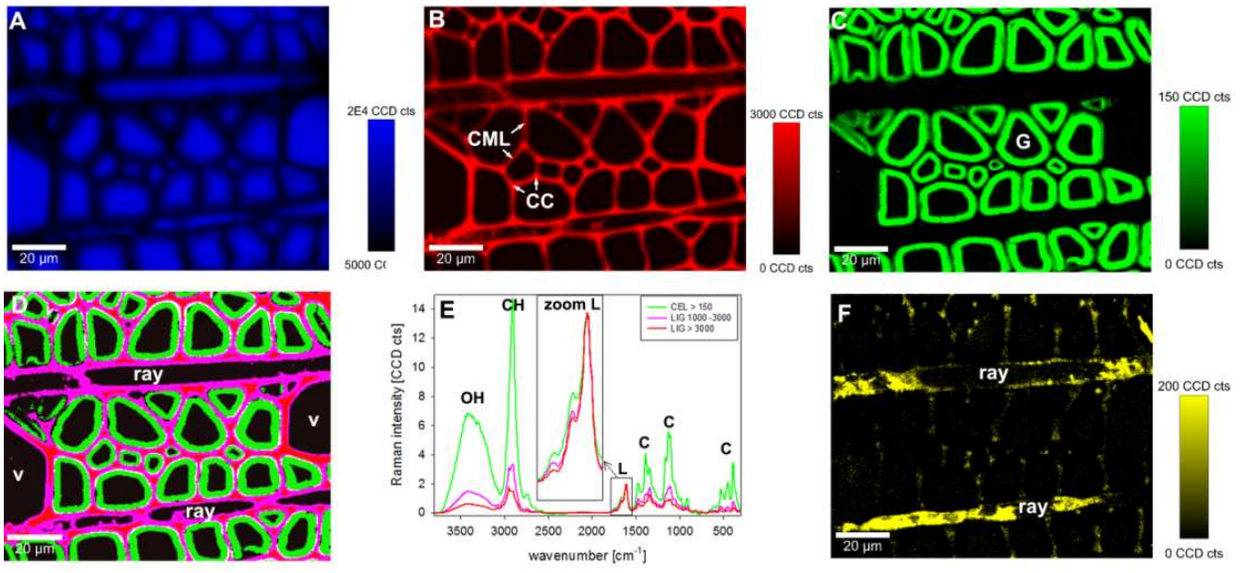

Figure 5. A-F: Raman images of poplar tension wood based on integrating the OH stretching region (A), the lignin marker band at about 1600 cm^{-1} (B) and the cellulose band at about 1388 cm^{-1} (C). In a combined image (D), regions with lignin intensity higher 3000 cts (red) and between 1000 and 3000 cts (pink) and with cellulose intensity >150 cts (green) are displayed. From these defined regions average spectra (baseline corrected and normalised to the 1600 cm^{-1} band) have been calculated (E). The content of the rays is visualized by integrating from 785-486 cm^{-1}. (Experimental: 532 nm excitation, 100x oil immersion objective, scan area: 120 µm x 100 µm, Pixels: 360x300, integration time: 0.4 s) (CC: cell corner, CML: compound middle lamella, G: gelatinous layer, v: vessel)

The example of poplar tension wood showed the potential of Raman imaging to get a detailed view on the molecular structure on the micron level. Distinguishing cell wall types based on their chemistry gives an overview of the tissue composition. Furthermore extracting the underlying Raman spectra for detailed analysis can elucidate specific insights into the molecular structure and composition. The position resolved micro-resolution opens up new ways for understanding biosynthesis (especially lignification) as gradients in developing tissues can be followed cell by cell and cellular components investigated together with the cell wall itself. Different performance and reactions upon treatment can be resolved on the cell wall level and help to understand recalcitrance of wood. Different species have different chemical composition and lignin structures and recently a clear distinction between pine and spruce in terms of the distribution of coniferyl alcohol and coniferyl aldehyde was recognized using the Raman imaging approach [170]. Furthermore changes due to environmental growth conditions or genetic engineering can be evaluated. By comparing lignification in wild-type and lignin-reduced 4CL transgenic *Populus trichocarpa* stem wood, it was shown that transgenic reduction of lignin is particularly pronounced in the S2 wall layer of fibres, suggesting that such transgenic approach may help overcome cell wall recalcitrance to wood saccharification [186]. A higher volume of

water was found in the cell wall of transgenic aspen compared with wild-type aspen, indicating an increase in the hydrophilicity of the cell wall [187].

5. Heterogeneity of lignin in the internode of the model grass *Brachypodium distachyon*

Grasses (or *Poaceae*, monocotyledon) are important plants on earth as they promote life and provide nutrients to both humans and animals. It is estimated that cereal grasses, i.e., corn, wheat, rice, oats, and barley, cover roughly 20% of the world's land surface and that the demand for these plants will remain high as the human population continues to increase [188]. Furthermore cereal grasses, including their grain and straw, are today not only used as sources of food but are also considered viable material for bioenergy. The grasses dedicated to biomass production, i.e., Switchgrass (*Panicum virgatum*) and Miscanthus (*Miscanthus sacchariflorus*, *M. sinensis* or *M. giganteus*) are mainly C4 plants that when grown in warm-environmental conditions, are more efficient in photosynthesis, nutrient-use and water-use [33]. The major limitations to the direct study of C4 grasses include the large size of the plants (requires land space), long generation times, and demanding growth requirements. Therefore several model plants, e.g., rice and more recently *Brachypdium distachyon*, were domesticated for laboratory studies (Figure 6A). *Brachypodium* now serves as an ideal experimental model for studying cereal grasses as it has many of the desirable traits for plant model systems including a small genome size, short generation time, the ability to self-pollinate, minimal input requirements and more importantly an amenability to forward and reverse genetic techniques [189]. Since 2001, *Brachypodium* has been established as a model however only recently have researchers begun to take advantage of this plant to study the monocot cell wall.

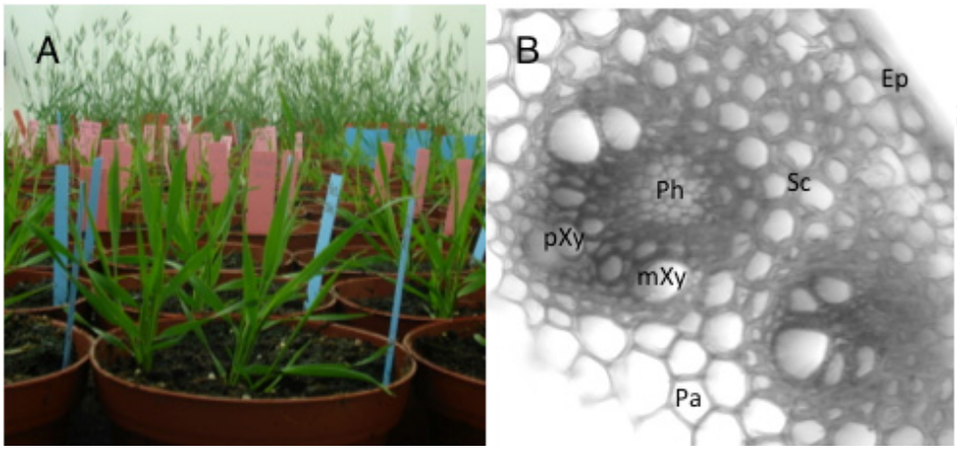

Figure 6. A-B: *Brachypodium distachyon*: Lateral view of *Brachypodium* development in the growth chamber (A). Cross section of a seven week old basal internode labelled with phloroglucinol-HCl (B). Dark labelling shows lignified cell walls. (Cell type abbreviations: Ep: epidermis; Sc: sclerenchyma; Ph: phloem; mXy: metaxylum; pXy: protoxylum; Pa: parenchyma)

The study of lignification in the monocot cell wall is of particular interest as several studies have demonstrated that lignin and phenolics bound to cell walls counter productively to saccharification yield and ruminant digestibility by reducing the accessibility of degrading/digestive enzymes to polysaccharides in the cell wall [45, 190]. Furthermore, a secondary, unintended effect of pre-treatments commonly used to reduce lignin content prior to saccharification for bioethanol production results in residual byproducts that inhibits growth of microorganisms used during fermentation. Therefore the natural resistance of lignocellulosic plant material to degradation serves as a major obstacle to efficient conversion of cellulose into fermentable sugars used for bioenergy [31, 191]. Within the monocot stems lignin is found in many tissues and cell types; the highest amount in the xylem tissue (Figure 6B). Phlorglucinol HCl staining gives insight into thevariability of lignification, but it is unspecific to different lignin and phenolic acid structures. As Raman images are based on underlying spectra, which represent a molecular fingerprint at every point within the acquired images, more detailed information can be gained.

Raman images of young (3 week old) basal internodes show point-wise accumulations of aromatic substances within the xylem tissues, while in the surrounding sclerenchyma fibres cell walls are visualized to be more homogenous (Figure 7A). In the lumen of the xylem cells remarkably high aromatic intensity is observed from deposits, which have not yet been further analysed. By integrating the marker band of ferulic acid at 1176 cm^{-1} (Figure 4B) again the point-wise accumulation within the xylem becomes visible, but less intensity is observed in the sclerenchyma fibres (Figure 7B). As stated previously grass cell walls contain high amounts of p-hydroxycinnamic acids, particularly ferulic (FA) and p-coumaric (pCA). Previous studies have demonstrated that both pCA and FA play an important functional role in the incorporation of lignin into the cell wall by aiding to establish ester or/and ether-linkages to cell wall polymers [192]. It was shown that ferulate esters act as initiation or nucleation sites of lignin deposition in grasses [193]. Ferulate molecules connect lignin to arabinoxylans primarily through ester-ether bonds and form dimeric structures cross-linking arabinoxylan chains to polysaccharides [194].

By integrating the carbohydrate band at about 903 cm^{-1}, slightly higher intensity in the sclerenchyma cells was observed (Figure 7C). On the contrary to the poplar wood cells (Figure 5A-F) no clear cell corners are seen within the young xylem and sclerenchyma fibres and differences in the distribution of aromatic and carbohydrate substances within the scanned cell wall area are less pronounced when applying the band integration approach for image calculation.

Nevertheless, a cluster analysis performed with derivatives of baseline corrected spectra reveals high heterogeneity of the spectra in the lumen and on the border of the cell walls (Figure 8A) as well as clear separation of the xylem cell wall and the sclerenchyma cell wall (Figure 8B). Based on the found clusters, average spectra can be calculated

corresponding to the separated regions. By this (Figure 8C-D) spectral (molecular) characterization of each cell wall region is possible on the micron level. Characteristic bands are observed e.g. for the lumen deposits (yellow line, Figure 8C), which can give insights into the chemical nature of these deposits. Furthermore, the gradual change recognized by the cluster analysis from the lumen towards the xylem cell wall can be analysed in detail. Comparing the xylem and sclerenchyma spectra (Figure 8D) it becomes clear that ferulic acid is much more accumulated in the xylem cells than in the surrounding sclerenchyma cells at this developmental stage of *Brachypodium*. The aryl stretching vibration as well as the marker bands at 1271 and 1176 cm^{-1} are clearly reduced in the spectrum corresponding to the sclerenchyma cells, whereas the carbohydrate distribution appears comparable (Figure 8D). The spot-wise pattern in the xylem was observed clearly by integrating the area of the bands (Figure 7A-B) and not in the cluster analysis (Figure 8B). Therefore it can be concluded that the spots reflect more changes in intensity (amount) than compositional (structural) changes. By studying the different cell wall types as well as cell lumen ingredients during different developmental stages, insights into lignification will be gained.

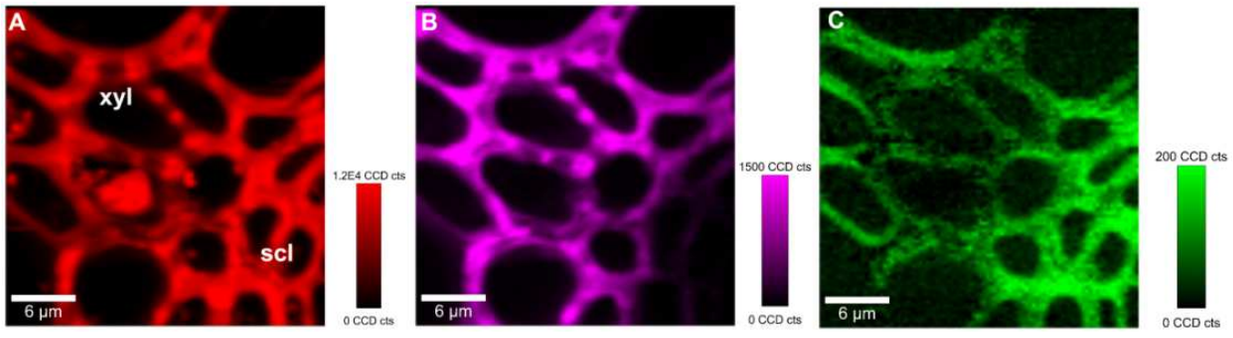

Figure 7. A-C: Raman images of a cross section of the basal internode of *Brachypodium distachyon* (three weeks old). High aromatic contribution is visualised by integrating from 1535 to 1674 cm^{-1} in the xylem (xyl) and surrounding sclerenchyma (scl) cells. When the typical band for ferulic acid at 1176 cm^{-1} is integrated (B) no lumen deposits are seen and less intensity in the sclerenchyma cells. The carbohydrate band at 903 cm^{-1} (925-887 cm^{-1}) shows higher intensity in the sclerenchyma cells (C). (Experimental: 532 nm excitation, 100x oil immersion objective, scan area: 30 µm x 30 µm, Pixels: 90x90, integration time: 0.3 s)

Recent Raman study on corn stover revealed that lignin and cellulose abundance varies significantly among different cell types: 5-times higher in sclerenchymea cells, 3-times higher in epidermal cells than bundle sheaths and parenchyma cells [177]. They also noted characteristic bands at 1428, 1271, and 1175 cm^{-1} in corn stover and although not assigned to ferulic acid, it seems that also in corn stover spectral contributions of ferulic acid have been reflected.

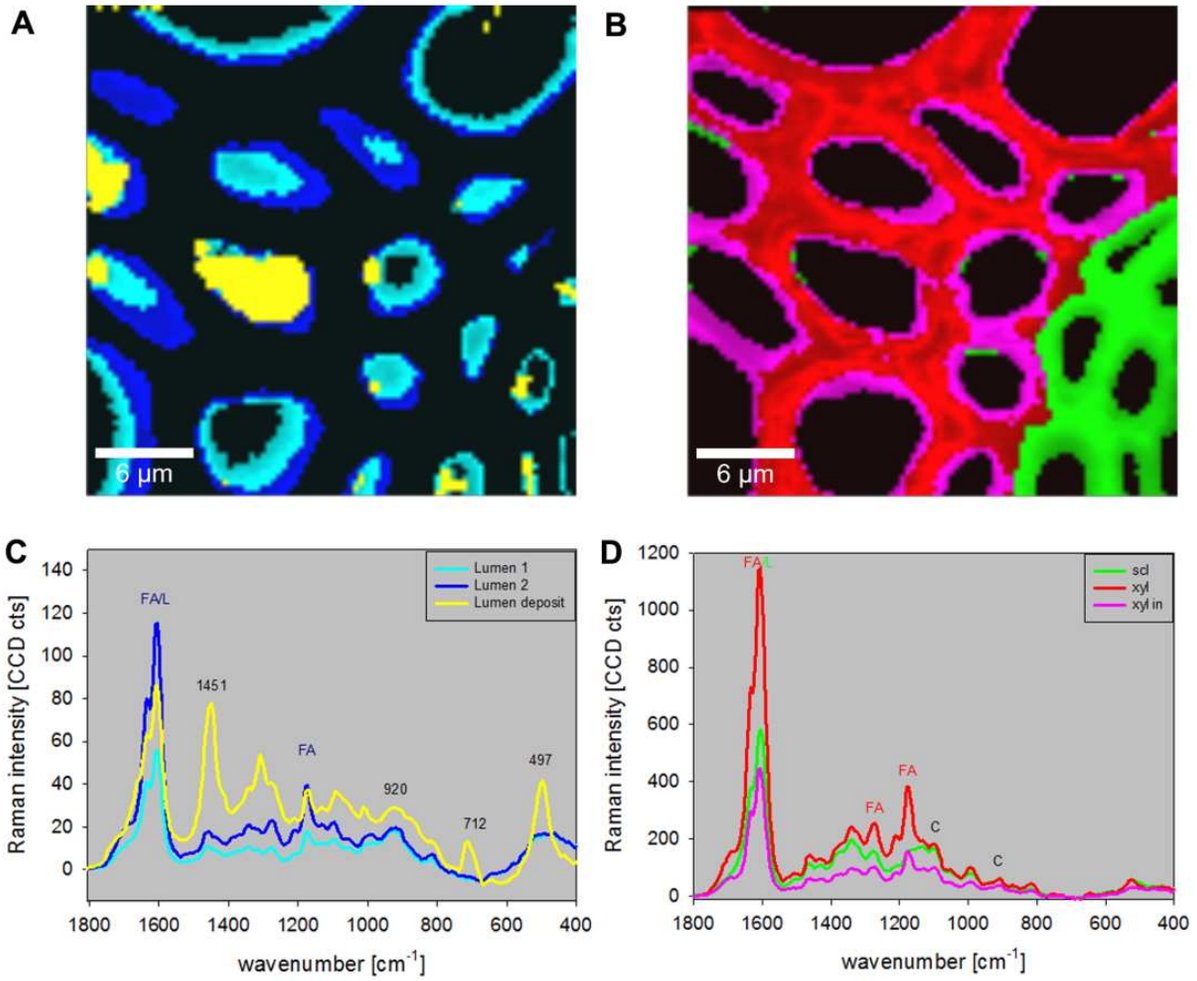

Figure 8. A-D: Raman images of *Brachypodium distachyon* based on a Cluster analysis using derivatives of baseline corrected spectra of the same measurement as shown in Figure 7. For clarity reasons the 6 calculated clusters are not shown within one image, but in two: A: representing the clusters of the cell lumen and borders towards the cell wall, B: the inner border of the xylem wall (pink) and the xylem wall itself (red) clearly separated from the sclerenchyma cells (green) High variability of the spectra within the cell lumen and its borders is seen (C) as well as clear differences between the sclerenchyma (scl) and xylem (xyl, xyl in) spectra (D).

6. Conclusion

The demand for plant biomass feedstock will increase as renewable resources get more and more attractive and further fields of utilizations open up. The mechanical performance as well as the recalcitrance of plant biomass to degradation is a function of which cell wall polymers are abundant and how they are cross-linked and aggregated within the walls. For understanding of biomass resources and an optimized utilization these higher order structures have to be probed in their native state on the micro- and nano level. The amount of cellulose as well as its crystallinity, structural arrangement (orientation) and interaction with other wood polymers play a key role in any utilization aspect. The recalcitrance to saccharification is a major limitation for conversion of lignocellulosic biomass to ethanol,

which is mainly due to the lignin content and composition. Therefore improving feedstocks for both animal consumption and for starting material for bioethanol production is proposed through breeding and genetic engineering of lignin. High throughput methods to characterize plant cell walls have become more and more important in order to follow the native variability as well as engineered changes. Both, FT-IR and Raman spectroscopy have given important insights into plant cell wall polymers during the last years. While Raman has the advantage of higher spatial resolution (<0.5 μm) to reveal changes on the cell wall layer level and the possibility of investigating the samples in the wet state, FT-IR is more sensitive to the functional group of hemicelluloses.

The examples of poplar tension wood and *Brachypodium* have shown the potential of Raman imaging to get a detailed view on the molecular structure on the micron level. Distinguishing cell wall types based on their chemistry gives an overview of the tissue composition. Furthermore extracting the underlying Raman spectra for detailed analysis can elucidate specific insights into the molecular structure and composition. The position resolved micro-resolution opens up new ways for understanding biosynthesis (especially lignification) as gradients in developing tissues can be followed cell by cell and cellular components investigated together with the cell wall itself. Different performance and reactions upon treatment can be resolved on the cell wall level and so-called *in-situ* approaches, watching directly the effect of treatment, will help to understand the performance (e.g. recalcitrance) of plant cell walls.

Author details

Notburga Gierlinger
BOKU - University of Natural Resources and Life Sciences,
Department of Material Sciences and Process Engineering, Vienna, Austria

Notburga Gierlinger and Tobias Keplinger
Johannes Kepler University Linz, Institute of Polymer Science, Linz, Austria

Michael Harrington
INRA, UMR 1318, Institut Jean Pierre Bourgin, France
AgroParisTech, Institut Jean Pierre Bourgin, France

Manfred Schwanninger
BOKU – University of Natural Resources and Life Sciences,
Department of Chemistry, Vienna, Austria

Acknowledgement

N.G. thanks Pierre Conchon and Catherine Coutand (INRA, Clermont Ferrand, France) for providing the poplar wood cross-section. MH is supported by the National Science Foundation (IRFP # 1002683).

7. References

[1] McKendry P (2002) Energy production from biomass (part 1): overview of biomass. Bioresour. Technol. 83(1): 37-46.
[2] Fengel D, Wegener G (1989) Wood: chemistry, ultrastructure, reactions. Berlin: Walter de Gruyter & Co., Berlin. 613 p.
[3] Salmén L, Burgert I (2009) Cell wall features with regard to mechanical performance. A review. Holzforschung 63: 121-129.
[4] Daniel G (2003) Microview of Wood under Degradation by Bacteria and Fungi. In: Goodell B, Nicholas DD, Schultz TP, editors. Wood Deterioration and Degradation. Advances in Our Changing World: ACS Symposium Series; p. 34 - 72.
[5] Zabel RA, Morrell JJ (1992) Wood Microbiology - Decay and its Prevention. Academic Press I, editor. San Diego: Academic Press, Inc. 476 p.
[6] Eriksson K-EL, Blanchette RA, Ander P (1990) Microbial and Enzymatic Degradation of Wood and Wood Components. Timell TE, editor. Berlin: Springer. 313 p.
[7] Goodell B (2003) Brown-Rot Fungal Degradation of Wood: Our Evolving View. In: Goodell B, Nicholas DD, Schultz TP, editors. Wood Deterioration and Degradation. Advances in Our Changing World: ACS Symposium Series; p. 97 - 118.
[8] Bajpai P (2012) Biotechnology for Pulp and Paper Processing. New York: Springer. 414 p.
[9] Mizrachi E, Mansfield SD, Myburg AA (2012) Cellulose factories: advancing bioenergy production from forest trees. New Phytol. 194(1): 54-62.
[10] Sims REH, Hastings A, Schlamadinger B, Taylor G, Smith P (2006) Energy crops: current status and future prospects. Global Change Biol 12(11): 2054-2076.
[11] Gordon GA (2011) Application of Fourier transform mid-infrared spectroscopy (FTIR) for research into biomass feed-stocks. In: Nikolic GS, editor. Fourier Transforms - New Analytical Approaches and FTIR Strategies. Rijeka, Croatia: lnTech; p. 71-88.
[12] Allison GG, Robbins MP, Carli J, Clifton-Brown J, Donnison I (2010) Designing biomass crops with improved calorific content and attributes for burning: a UK perspective. In: P. Mascia, Schefrran J, Widhalm JM, editors. Plant Biotechnology for Sustainable Production of Energy and CoProducts. Heidelberg, Germany: Springer; p. 25-56.
[13] McCarthy JL, Islam A (2000) Lignin chemistry, technology, and utilization: A brief history. In: Glasser WG, Northey RA, Schultz TP, editors. Lignin : Historical, Biological, and Materials Perspectives: American Chemical Society; p. 2-99.
[14] Ko JH, Kim HT, Han KH (2011) Biotechnological improvement of lignocellulosic feedstock for enhanced biofuel productivity and processing. Plant Biotechnol. Rep. 5(1): 1-7.
[15] Kishimoto T (2009) Synthesis of lignin model compounds and their application to wood research. Mokuzai Gakkaishi 55(4): 187-197.
[16] Holmgren A, Norgren M, Zhang L, Henriksson G (2009) On the role of the monolignol gamma-carbon functionality in lignin biopolymerization. Phytochemistry 70(1): 147-155.

[17] Hafren J, Westermark U, Lennholm H, Terashima N (2002) Formation of C-13-enriched cell-wall DHP using isolated soft xylem from *Picea abies*. Holzforschung 56(6): 585-591.
[18] Monties B (2005) Biological variability of lignin. Cell. Chem. Technol. 39(5-6): 341-367.
[19] Zhong RQ, Morrison WH, Himmelsbach DS, Poole FL, Ye Z-H (2000) Essential role of caffeoyl coenzyme A *O*-methyltransferase in lignin biosynthesis in woody poplar plants. Plant Physiol. 124(2): 563-577.
[20] Liu CJ (2012) Deciphering the enigma of lignification: Precursor transport, oxidation, and the topochemistry of lignin assembly. Mol Plant 5(2): 304-317.
[21] Marjamaa K, Kukkola EM, Fagerstedt KV (2009) The role of xylem class III peroxidases in lignification. J. Exp. Bot. 60(2): 367-376.
[22] Chen YR, Sarkanen S (2010) Macromolecular replication during lignin biosynthesis. Phytochemistry 71(4): 453-462.
[23] Baucher M, Monties B, Van Montagu M, Boerjan W (1998) Biosynthesis and genetic engineering of lignin. Crit. Rev. Plant Sci. 17(2): 125-197.
[24] Whetten R, Sederoff R (1995) Lignin biosynthesis. Plant Cell 7: 1001-1013.
[25] Umezawa T (2010) The cinnamate/monolignol pathway. Phytochem. Rev. 9(1): 1-17.
[26] Vanholme R, Demedts B, Morreel K, Ralph J, Boerjan W (2010) Lignin biosynthesis and structure. Plant Physiol. 153(3): 895-905.
[27] Wang C, Wang YC, Diao GP, Jiang J, Yang CP (2010) Isolation and characterization of expressed sequence tags (ESTs) from cambium tissue of birch (*Betula platyphylla* Suk). Plant Mol. Biol. Rep. 28(3): 438-449.
[28] Samuels AL, Rensing KH, Douglas CJ, Mansfield SD, Dharmawardhana DP, Ellis BE (2002) Cellular machinery of wood production: differentiation of secondary xylem in *Pinus contorta* var. *latifolia*. Planta 216(1): 72-82.
[29] Studer MH, DeMartini JD, Davis MF, Sykes RW, Davison B, Keller M, Tuskan GA, Wyman CE (2011) Lignin content in natural Populus variants affects sugar release. P. Natl. Acad. Sci. USA 108(15): 6300-6305.
[30] Grabber JH (2005) How do lignin composition, structure, and cross-linking affect degradability? A review of cell wall model studies. Crop Sci. 45(3): 820-831.
[31] Carroll A, Somerville C (2009) Cellulosic biofuels. Annu. Rev. Plant Biol. 60: 165-182.
[32] Chang MCY (2007) Harnessing energy from plant biomass. Curr. Opin. Chem. Biol. 11(6): 677-684.
[33] Clifton-Brown J, Robson P, Allison G, Lister S, Sanderson R, Hodgson E, Farrar K, Hawkins S, Jensen E, Jones S, Huang L, Roberts P, Youell S, Jones B, Wright A, Valantine J, Donnison I (2008) Miscanthus: breeding our way to a better future. In: E. Booth, M. Green, A. Karp, I. Shield, D. Stock, Turley D, editors. Biomass and Energy Crops III. Warwick, UK: Association of Applied Biologists; p. 199-206.
[34] Hodgson EM, Fahmi R, Yates N, Barraclough T, Shield I, Allison G, Bridgwater AV, Donnison IS (2010) *Miscanthus* as a feedstock for fast-pyrolysis: Does agronomic treatment affect quality? Bioresour. Technol. 101(15): 6185-6191.
[35] Hodgson EM, Lister SJ, Bridgwater AV, Clifton-Brown J, Donnison IS (2010) Genotypic and environmentally derived variation in the cell wall composition of *Miscanthus* in relation to its use as a biomass feedstock. Biomass. Bioenerg. 34(5): 652-660.

[36] Boudet AM, Grima-Pettenati J (1996) Lignin genetic engineering. Mol. Breeding 2(1): 25-39.
[37] Boudet AM, Lapierre C, Grima-Pettenati J (1995) Tansley review No-80 - Biochemistry and molecular-biology of lignification. New Phytol. 129(2): 203-236.
[38] Chiang VL (2006) Monolignol biosynthesis and genetic engineering of lignin in trees, a review. Environ. Chem. Lett. 4(3): 143-146.
[39] Harris D, DeBolt S (2010) Synthesis, regulation and utilization of lignocellulosic biomass. Plant Biotechnol. J. 8(3): 244-262.
[40] Higuchi T (2000) The present state and problems in lignin biosynthesis. Cell. Chem. Technol. 34(1-2): 79-100.
[41] Horvath B, Peszlen I, Peralta P, Kasal B, Li LG (2010) Effect of lignin genetic modification on wood anatomy of Aspen trees. Iawa J. 31(1): 29-38.
[42] Koehler L, Telewski FW (2006) Biomechanics and transgenic wood. Am. J. Bot. 93(10): 1433-1438.
[43] Leple JC, Dauwe R, Morreel K, Storme V, Lapierre C, Pollet B, Naumann A, Kang KY, Kim H, Ruel K, Lefebvre A, Joseleau JP, Grima-Pettenati J, De Rycke R, Andersson-Gunneras S, Erban A, Fehrle I, Petit-Conil M, Kopka J, Polle A, Messens E, Sundberg B, Mansfield SD, Ralph J, Pilate G, Boerjan W (2007) Downregulation of cinnamoyl-coenzyme a reductase in poplar: Multiple-level phenotyping reveals effects on cell wall polymer metabolism and structure. Plant Cell 19(11): 3669-3691.
[44] Pu YQ, Chen F, Ziebell A, Davison BH, Ragauskas AJ (2009) NMR characterization of C3H and HCT down-regulated alfalfa lignin. Bioenerg. Res. 2(4): 198-208.
[45] Chen F, Dixon RA (2007) Lignin modification improves fermentable sugar yields for biofuel production. Nat Biotechnol. 25(7): 759-761.
[46] Maunu SL (2002) NMR studies of wood and wood products. Prog. Nucl. Magn. Reson. Spectrosc. 40: 151-174.
[47] Lu F, Ralph J (2003) Non-degradative dissolution and acetylation of ball-milled plant cell walls: high-resolution solution-state NMR. Plant J. 35: 535-544.
[48] Yelle DJ, Ralph J, Li F, Hammel KE (2008) Evidence for cleavage of lignin by a brown rot basidiomycete. Environ. Microbiol. 10(7): 1844-1849.
[49] Yelle DJ, Wei D, Ralph J, Hammel KE (2011) Multidimensional NMR analysis reveals truncated lignin structures in wood decayed by the brown rot basidiomycete *Postia placenta*. Environ. Microbiol. 13(4): 1091-1100.
[50] Alves A, Schwanninger M, Pereira H, Rodrigues J (2006) Analytical pyrolysis as a direct method to determine the lignin content in wood - Part 1: Comparison of pyrolysis lignin with Klason lignin. J. Anal. Appl. Pyrol. 76(1-2): 209-213.
[51] Alves A, Gierlinger N, Schwanninger M, Rodrigues J (2009) Analytical pyrolysis as a direct method to determine the lignin content in wood Part 3. Evaluation of species-specific and tissue-specific differences in softwood lignin composition using principal component analysis. J. Anal. Appl. Pyrol. 85(1-2): 30-37.
[52] Anterola AM, Lewis NG (2002) Review: Trends in lignin modification: a comprehensive analysis of the effects of genetic manipulations/mutations on lignification and vascular integrity. Phytochemistry 61: 221–294.

[53] Korosec RC, Lavric B, Rep G, Pohleven F, Bukovec P (2009) Thermogravimetry as a possible tool for determining modification degree of thermally treated Norway spruce wood. J. Therm. Anal. Calorim. 98(1): 189-195.
[54] Taneda K, Nishiyama Y, Uparivong S (1995) An evaluation of kinetic-parameters by derivative thermogravimetry and Its application to oood and other bioresources. Mokuzai Gakkaishi 41(4): 414-424.
[55] Gindl W, Grabner M (2000) Characteristics of spruce [*Picea abies* (L.) Karst] latewood formed under abnormally low temperatures. Holzforschung 54(1): 9-11.
[56] Gindl W, Grabner M, Wimmer R (2000) The influence of temperature on latewood lignin content in treeline Norway spruce compared with maximum density and ring width. Trees-Struct. Funct. 14(7): 409-414.
[57] Griffiths PR, Haseth JAD (2007) Fourier Transform Infrared Spectrometry. 2nd ed. New York: Wiley. 529 p.
[58] Schrader B (1995) Infrared and Raman Spectroscopy: Methods and Applications. Weinheim: Wiley-VCH Verlag GmbH 788 p.
[59] Tsuchikawa S (2007) A review of recent near infrared research for wood and paper. Appl. Spectrosc. Rev. 42: 43-71.
[60] Tsuchikawa S, Schwanninger M (2011) A review of recent near infrared research for wood and paper (Part 2). Appl. Spectrosc. Rev. (in print): DOI: 10.1080/05704928.05702011.05621079.
[61] Schwanninger M, Rodrigues J, Fackler K (2011) A review of band assignments in near infrared spectra of wood and wood components. J. Near Infrared Spectrosc. 19(287-308).
[62] Schwanninger M, Hinterstoisser B, Gradinger C, Messner K, Fackler K (2004) Examination of spruce wood biodegraded by *Ceriporiopsis subvermispora* using near and mid infrared spectroscopy. J. Near Infrared Spectrosc. 12(6): 397-409.
[63] Fackler K, Schmutzer M, Manoch L, Schwanninger M, Hinterstoisser B, Ters T, Messner K, Gradinger C (2007) Evaluation of the selectivity of white rot isolates using near infrared spectroscopic techniques. Enzyme Microb. Technol. 41: 881-887.
[64] Fackler K, Schwanninger M, Gradinger C, Srebotnik E, Hinterstoisser B, Messner K (2007) Fungal decay of spruce and beech wood assessed by near infrared spectroscopy in combination with uni- and multivariate data analysis. Holzforschung 62: 223-230.
[65] Fackler K, Gradinger C, Hinterstoisser B, Messner K, Schwanninger M (2006) Lignin degradation by white rot fungi on spruce wood shavings during short-time solid-state fermentations monitored by near infrared spectroscopy. Enzyme Microb. Technol. 39(7): 1476-1483.
[66] Fackler K, Schwanninger M (2010) Polysaccharide degradation and lignin modification during brown-rot of spruce wood: a polarised Fourier transfrom near infrared study. J. Near Infrared Spectrosc. 18: 403-416.
[67] Fackler K, Schwanninger M (2011) Accessibility of hydroxyl groups of brown-rot degraded spruce wood to heavy water. J. Near Infrared Spectrosc. 19: 359-368.
[68] Fackler K, Schwanninger M, Gradinger C, Hinterstoisser B, Messner K (2007) Qualitative and quantitative changes of beech wood degraded by wood rotting

basidiomycetes monitored by Fourier transform infrared spectroscopic methods and multivariate data analysis. FEMS Microbiol. Lett. 271: 162-169.
[69] Åkerholm M, Salmén L (2001) Interactions between wood polymers studied by dynamic FT-IR spectroscopy. Polymer 42: 963-969.
[70] Åkerholm M, Salmén L (2003) The oriented structure of lignin and its viscoelastic properties studied by static and dynamic FT-IR spectroscopy. Holzforschung 57(5): 459-465.
[71] Hinterstoisser B, Åkerholm M, Salmén L (2001) Effect of fiber orientation in dynamic FTIR study on native cellulose. Carbohydr. Res. 334: 27-37.
[72] Hinterstoisser B, Salmén L (2000) Application of dynamic 2D FTIR to cellulose. Vib. Spectrosc. 22(1-2): 111-118.
[73] Stevanic JS, Salmén L (2008) Characterizing wood polymers in the primary cell wall of Norway spruce (*Picea abies* (L.) Karst.) using dynamic FT-IR spectroscopy. Cellulose 15(2): 285-295.
[74] Stevanic JS, Salmén L (2009) Orientation of the wood polymers in the cell wall of spruce wood fibres. Holzforschung 63(5): 497-503.
[75] Atalla RH, Agarwal UP (1985) Raman microprobe evidence for lignin orientation in the cell walls of native woody tissue. Science 227: 636-638.
[76] Chowdhury S, Madsen LA, Frazier CE (2012) Probing alignment and phase behavior in intact wood cell walls using H-2 NMR spectroscopy. Biomacromolecules 13(4): 1043-1050.
[77] Salmén L, Olsson A-M, Stevanic JS, Simonovic J, Radotic K (2012) Structural organization of the wood polymers in the wood fibre structure Bioresources 7(1): 521-532.
[78] Gierlinger N, Goswami L, Schmidt M, Burgert I, Coutand C, Rogge T, Schwanninger M (2008) *In situ* FT-IR microscopic study on enzymatic treatment of poplar wood cross-sections. Biomacromolecules 9: 2194-2201.
[79] Chen LM, Carpita NC, Reiter WD, Wilson RH, Jeffries C, McCann MC (1998) A rapid method to screen for cell-wall mutants using discriminant analysis of Fourier transform infrared spectra. Plant J. 16(3): 385-392.
[80] Mouille G, Robin S, Lecomte M, Pagant S, Hofte H (2003) Classification and identification of *Arabidopsis* cell wall mutants using Fourier-Transform InfraRed (FT-IR) microspectroscopy. Plant J. 35(3): 393-404.
[81] Robin S, Lecomte M, Hofte H, Mouille G (2003) A procedure for the clustering of cell wall mutants in the model plant *Arabidopsis* based on Fourier-transform infrared (FT-IR) spectroscopy. J. Appl. Stat. 30(6): 669-681.
[82] McCann MC, Defernez M, Urbanowicz BR, Tewari JC, Langewisch T, Olek A, Wells B, Wilson RH, Carpita NC (2007) Neural network analyses of infrared spectra for classifying cell wall architectures. Plant Physiol. 143(3): 1314-1326.
[83] Fackler K, Stevanic JS, Ters T, Hinterstoisser B, Schwanninger M, Salmén L (2010) Localisation and characterisation of incipient brown-rot decay within spruce wood cell walls using FT-IR imaging microscopy. Enzyme Microb. Technol. 47: 257-267.

[84] Fackler K, Stevanic JS, Ters T, Hinterstoisser B, Schwanninger M, Salmén L (2011) FT-IR imaging microscopy to localise and characterise simultaneous and selective white-rot decay within spruce wood cells. Holzforschung 65: 411-420.
[85] Smith E, Dent G (2005) Modern Raman Spectroscopy - A practical approach. Manchester: John Wiley & Sons Ltd. 210 p.
[86] Landsberg G, Mandelstam L (1928) Light scattering in crystals. Zeitschrift Für Physik 50(11-12): 769-780.
[87] Raman CV, Krishnan KS (1928) A new type of secondary radiation. Nature 121: 501-502.
[88] Hirschfeld T, Chase B (1986) FT-Raman spectroscopy - development and justification. Appl. Spectrosc. 40(2): 133-137.
[89] Das RS, Agrawal YK (2011) Raman spectroscopy: Recent advancements, techniques and applications. Vib. Spectrosc. 57(2): 163-176.
[90] Hollricher O (2010) Raman Instrumentation for Confocal Raman Microscopy. In: Diening T, Hollricher O, Toporski J, editors. Confocal Raman microscopy. Berlin Heidelberg: Springer-Verlag; p. 43-60.
[91] Dieing T, Hollricher O (2008) High-resolution, high-speed confocal Raman imaging. Vib. Spectrosc. 48(1): 22-27.
[92] Withnall R, Chowdhry BZ, Silver J, Edwards HGM, de Oliveira LFC (2003) Raman spectra of carotenoids in natural products. Spectroc. Acta Pt. A-Molec. Biomolec. Spectr. 59: 2207-2212.
[93] Saariaho AM, Jääskeläinen AS, Matousek P, Towrie M, Parker AW, Vuorinen T (2004) Resonance Raman spectroscopy of highly fluorescing lignin containing chemical pulps: Suppression of fluorescence with an optical Kerr gate. Holzforschung 58(1): 82-90.
[94] Matousek P, Towrie M, Stanley A, Parker AW (1999) Efficient rejection of fluorescence from Raman spectra using picosecond Kerr gating. Appl. Spectrosc. 53(12): 1485-1489.
[95] Matousek P, Towrie M, Parker AW (2002) Fluorescence background suppression in Raman spectroscopy using combined Kerr gated and shifted excitation Raman difference techniques. J. Raman Spectrosc. 33: 238-242.
[96] Sharma B, Frontiera RR, Henry AI, Ringe E, Van Duyne RP (2012) SERS: Materials, applications, and the future. Mater. Today 15(1-2): 16-25.
[97] Zhang Y, Hong H, Myklejord DV, Cai WB (2011) Molecular imaging with SERS-active nanoparticles. Small 7(23): 3261-3269.
[98] McNay G, Eustace D, Smith WE, Faulds K, Graham D (2011) Surface-Enhanced Raman Scattering (SERS) and Surface-Enhanced Resonance Raman Scattering (SERRS): A review of applications. Appl. Spectrosc. 65(8): 825-837.
[99] Rösch P, Popp J, Kiefer W (1999) Raman and surface enhanced Raman spectroscopic investigation on Lamiaceae plants. J. Mol. Struct. 481: 121-124.
[100] Cheng JX, Xie XS (2004) Coherent anti-Stokes Raman scattering microscopy: Instrumentation, theory, and applications. J. Phys. Chem. B 108(3): 827-840.
[101] Chen JX, Volkmer A, Book LD, Xie XS (2002) Multiplex coherent anti-stokes Raman scattering microspectroscopy and study of lipid vesicles. J. Phys. Chem. B 106(34): 8493-8498.

[102] Le TT, Yue SH, Cheng JX (2010) Shedding new light on lipid biology with coherent anti-Stokes Raman scattering microscopy. J. Lipid Res. 51(11): 3091-3102.

[103] Pezacki JP, Blake JA, Danielson DC, Kennedy DC, Lyn RK, Singaravelu R (2011) Chemical contrast for imaging living systems: molecular vibrations drive CARS microscopy. Nat. Chem. Biol. 7(3): 137-145.

[104] Fu D, Lu FK, Zhang X, Freudiger C, Pernik DR, Holtom G, Xie XS (2012) Quantitative chemical imaging with multiplex stimulated Raman scattering microscopy. J. Am. Chem. Soc. 134(8): 3623-3626.

[105] Mallick B, Lakhsmanna A, Umapathy S (2011) Ultrafast Raman loss spectroscopy (URLS): instrumentation and principle. J. Raman Spectrosc. 42(10): 1883-1890.

[106] Freudiger CW, Min W, Holtom GR, Xu BW, Dantus M, Xie XS (2011) Highly specific label-free molecular imaging with spectrally tailored excitation-stimulated Raman scattering (STE-SRS) microscopy. Nat. Photonics 5(2): 103-109.

[107] [107] Saar BG, Zeng YN, Freudiger CW, Liu YS, Himmel ME, Xie XS, Ding SY (2010) Label-free, real-time monitoring of biomass processing with stimulated Raman scattering microscopy. Angew. Chem.-Int. Edit. 49(32): 5476-5479.

[108] [108] Griffith PR (2009) Infrared and Raman Instrumentation for Mapping and Imaging. In: Salzer R, Siesler HW, editors. Infrared and Raman Spectroscopic Imaging. Weinheim: Wiley-VCH Verlag GmbH & Co. KGaA; p. 3-64.

[109] Everall N, Lapham J, Adar F, Whitley A, Lee E, Mamedov S (2007) Optimizing depth resolution in Confocal Raman microscopy: A comparison of metallurgical, dry corrected, and oil immersion objectives. Appl. Spectrosc. 61(3): 251-259.

[110] Bruneel JL, Lassegues JC, Sourisseau C (2002) In-depth analyses by confocal Raman microspectrometry: experimental features and modeling of the refraction effects. J. Raman Spectrosc. 33(10): 815-828.

[111] Verma P, Ichimura T, Yano T, Saito Y, Kawata S (2010) Nano-imaging through tip-enhanced Raman spectroscopy: Stepping beyond the classical limits. Laser Photon. Rev. 4(4): 548-561.

[112] Deckert-Gaudig T, Deckert V (2011) Nanoscale structural analysis using tip-enhanced Raman spectroscopy. Curr. Opin. Chem. Biol. 15(5): 719-724.

[113] Elfick APD, Downes AR, Mouras R (2010) Development of tip-enhanced optical spectroscopy for biological applications: a review. Anal. Bioanal. Chem. 396(1): 45-52.

[114] Nelson MP, Treado PJ (2010) Raman imaging instrumentation. In: Sasic S, Ozaki Y, editors. Raman, Infrared, and Near-Infrared Chemical Imaging. Hoboken, New Jersey: John Wiley & Sons, Inc.; p. 23-55.

[115] Toytman I, Simanovskii D, Palanker D (2009) On illumination schemes for wide-field CARS microscopy. Opt. Express 17(9): 7339-7347.

[116] Schlucker S, Schaeberle MD, Huffman SW, Levin IW (2003) Raman microspectroscopy: A comparison of point, line, and wide-field imaging methodologies. Anal. Chem. 75(16): 4312-4318.

[117] McCreery RL (2000) Raman microscopy and imaging. In: Winefordner JD, editor. Raman Spectroscopy for Chemical Analysis. New York: John Wiley & Sons, Inc.; p. 293-332.

[118] Gamsjaeger S, Kazanci M, Paschalis EP, Fratzl P (2009) Raman application in bone imaging. In: Amer MS, editor. Raman Spectroscopy for soft matter applications. New Jersey: Wiley VCH; p. 227–267.
[119] Gierlinger N, Keplinger T, Harrington M (2012) Imaging of plant cell walls by Confocal Raman microscopy. Nat. Protoc.: in review.
[120] Zhang DM, Jallad KN, Ben-Amotz D (2001) Stripping of cosmic spike spectral artifacts using a new upper-bound spectrum algorithm. Appl. Spectrosc. 55(11): 1523-1531.
[121] Katsumoto Y, Ozaki Y (2003) Practical algorithm for reducing convex spike noises on a spectrum. Appl. Spectrosc. 57(3): 317-322.
[122] Diening T, Ibach W (2010) Software Requirements and Data Analysis in Confocal Raman Microscopy. In: Diening T, Hollricher O, Toporski J, editors. Confocal Raman microscopy. Berlin Heidelberg: Springer-Verlag; p. 61-89.
[123] Savitzky A, Golay MJE (1964) Smoothing and differentiation of data by simplified least squares procedures. Anal. Chem. 36: 1627 - 1639.
[124] Ramos PM, Ruisanchez I (2005) Noise and background removal in Raman spectra of ancient pigments using wavelet transform. J. Raman Spectrosc. 36(9): 848-856.
[125] Liland KH, Rukke EO, Olsen EF, Isaksson T (2011) Customized baseline correction. Chemometrics Intell. Lab. Syst. 109(1): 51-56.
[126] de Juan A, Maeder M, Hancewicz T, Duponchel L, Tauler R (2009) Chemometric Tools for Image Analysis. In: Salzer R, W. SH, editors. Infrared and Raman Spectroscopic Imaging. Weinheim: WILEY-VCH Verlag GmbH & Co. KGaA; p. 65-108.
[127] Schulze G, Jirasek A, Yu MML, Lim A, Turner RFB, Blades MW (2005) Investigation of selected baseline removal techniques as candidates for automated implementation. Appl. Spectrosc. 59(5): 545-574.
[128] Prakash BD, Wei YC (2011) A fully automated iterative moving averaging (AIMA) technique for baseline correction. Analyst 136(15): 3130-3135.
[129] Schulze HG, Foist RB, Okuda K, Ivanov A, Turner RFB (2011) A model-free, fully automated baseline-removal method for Raman spectra. Appl. Spectrosc. 65(1): 75-84.
[130] Zhang ZM, Chen S, Liang YZ (2010) Baseline correction using adaptive iteratively reweighted penalized least squares. Analyst 135(5): 1138-1146.
[131] Schmidt U, Ibach W, Muller J, Weishaupt K, Hollricher O (2006) Raman spectral imaging - A nondestructive, high resolution analysis technique for local stress measurements in silicon. Vib. Spectrosc. 42(1): 93-97.
[132] Geladi P, Grahn H, Manley M (2010) Data analysis and chemometrics for hyperspectral Imaging. In: Sasic S, Ozaki Y, editors. Raman, Infrared, and Near-Infrared Chemical Imaging. Hoboken, New Jersey: John Wiley & Sons, Inc.; p. 93-109.
[133] Shinzawa H, Awa K, Kanematsu W, Ozaki Y (2009) Multivariate data analysis for Raman spectroscopic imaging. J. Raman Spectrosc. 40(12): 1720-1725.
[134] Næs T, Isaksson T, Fearn T, Davies T (2002) A User-Friendly Guide to Multivariate Calibration and Classification. first ed. Chichester: NIR Publications. 344 p.
[135] Geladi P (2003) Chemometrics in spectroscopy. Part 1. Classical chemometrics. Spectroc. Acta Pt. B-Atom. Spectr. 58: 767-782.

[136] Hastie T, Tibshirani R, Friedman J (2009) The Elements of Statistical Learning. New York: Springer. 739 p.
[137] Cosgrove DJ (2005) Growth of the plant cell wall. Nat. Rev. Mol. Cell Biol. 6(11): 850-861.
[138] Wiley JH, Atalla RH (1987) Band assignments in the Raman spectra of celluloses. Carbohydr. Res. 160: 113-129.
[139] Agarwal UP, Atalla RH (1986) In-situ Raman microprobe studies of plant cell walls - Macromolecular organization and compositional variability in the secondary wall of *Picea mariana* (Mill) Bsp. Planta 169(3): 325-332.
[140] Atalla RH, Agarwal UP (1986) Recording Raman-spectra from plant cell walls. J. Raman Spectrosc. 17(2): 229-231.
[141] Schenzel K, Fischer S (2001) NIR FT Raman spectroscopy - a rapid analytical tool for detecting the transformation of cellulose polymorphs. Cellulose 8(1): 49-57.
[142] Gierlinger N, Luss S, Konig C, Konnerth J, Eder M, Fratzl P (2010) Cellulose microfibril orientation of *Picea abies* and its variability at the micron-level determined by Raman imaging. J. Exp. Bot. 61(2): 587-595.
[143] Agarwal UP, Reiner RS, Ralph SA (2010) Cellulose I crystallinity determination using FT-Raman spectroscopy: univariate and multivariate methods. Cellulose 17(4): 721-733.
[144] Agarwal UP, Ralph SA (1997) FT-Raman spectroscopy of wood: Identifying contributions of lignin and carbohydrate polymers in the spectrum of black spruce (*Picea mariana*). Appl. Spectrosc. 51(11): 1648-1655.
[145] Himmelsbach DS, Khahili S, Akin DE (1999) Near-infrared–Fourier-transform–Raman microspectroscopic imaging of flax stems. Vib. Spectrosc. 19: 361-367.
[146] Chu LQ, Masyuko R, Sweedler JV, Bohn PW (2009) Base-induced delignification of Miscanthus x giganteus studied by three-dimensional confocal Raman imaging. Bioresour. Technol. 101(13): 4919-4925.
[147] Mathlouthi M, Koenig JL (1986) Vibrational Spectra of Carbohydrates. Adv. Carbohydr. Chem. Biochem. 44: 7-89.
[148] Richter S, Mussig J, Gierlinger N (2011) Functional plant cell wall design revealed by the Raman imaging approach. Planta 233(4): 763-772.
[149] Gierlinger N, Sapei L, Paris O (2008) Insights into the chemical composition of *Equisetum hyemale* by high resolution Raman imaging. Planta 227(5): 969-980.
[150] Synytsya A, Copikova J, Matejka P, Machovic V (2003) Fourier transform Raman and infrared spectroscopy of pectins. Carbohydr. Polym. 54(1): 97-106.
[151] Arjyal BP, Katerelos DG, Filiou C, Galiotis C (2000) Measurement and Modeling of Stress Concentration around a Circular Notch. Exp. Mech. 40(3): 248-255.
[152] Lewis NG, Yamamoto E (1990) Lignin: occurrence, biogenesis and biodegradation. Annu. Rev. Plant Physiol. Plant Mol. Biol. 41: 455-496.
[153] Barsberg S, Matousek P, Towrie M (2005) Structural analysis of lignin by resonance Raman spectroscopy. Macromol. Biosci. 5(8): 743-752.
[154] Perera PN, Schmidt M, Chiang VL, Schuck PJ, Adams PD (2012) Raman-spectroscopy-based noninvasive microanalysis of native lignin structure. Anal. Bioanal. Chem. 402(2): 983-987.

[155] Agarwal UP, Atalla RH (1994) Raman spectral features associated with chromophores in high-yield pulps. J. Wood Chem. Technol. 14(2): 227-241.

[156] Agarwal UP (1999) An Overview of Raman Spectroscopy as Applied to Lignocellulosic Materials. In: Argyropoulos DS, editor. Advances in Lignocellulosics Characterization. Atlanta, GA: TAPPI Press; p. 209-225.

[157] Agarwal UP, Landucci LL (2004) FT-Raman investigation of bleaching of spruce thermornechanical pulp. J. Pulp Pap. Sci. 30(10): 269-274.

[158] Stewart D, Yahiaoui N, McDougall GJ, Myton K, Marque C, Boudet AM, Haigh J (1997) Fourier-transform infrared and Raman spectroscopic evidence for the incorporation of cinnamaldehydes into the lignin of transgenic tobacco (*Nicotiana tabacum* L) plants with reduced expression of cinnamyl alcohol dehydrogenase. Planta 201(3): 311-318.

[159] Himmelsbach DS, Akin DE (1998) Near-infrared Fourier-transform Raman spectroscopy of flax (Linum usitatissimum L.) stems. J. Agric. Food Chem. 46(3): 991-998.

[160] Ona T, Sonoda T, Ito K, Shibata M, Katayama T, Kato T, Ootake Y (1998) Non-destructive determination of lignin syringyl/guaiacyl monomeric composition in native wood by Fourier transform Raman spectroscopy. J. Wood Chem. Technol. 18(1): 43-51.

[161] Sun L, Varanasi P, Yang F, Loque D, Simmons BA, Singh S (2012) Rapid determination of syringyl:guaiacyl ratios using FT-Raman spectroscopy. Biotechnol. Bioeng. 109(3): 647-656.

[162] Barsberg S, Matousek P, Towrie M, Jorgensen H, Felby C (2006) Lignin radicals in the plant cell wall probed by Kerr-gated resonance Raman spectroscopy. Biophys. J. 90(8): 2978-2986.

[163] Saariaho AM, Jääskeläinen AS, Nuopponen M, Vuorinen T (2003) Ultra violet resonance Raman spectroscopy in lignin analysis: determination of characteristic vibrations of p-hydroxyphenyl, guaiacyl, and syringyl lignin structures. Appl. Spectrosc. 57(1): 58-66.

[164] Jääskeläinen AS, Saariaho AM, Vyorykka J, Vuorinen T, Matousek P, Parker AW (2006) Application of UV-Vis and resonance Raman spectroscopy to study bleaching and photoyellowing of thermomechanical pulps. Holzforschung 60(3): 231-238.

[165] Zeng Y, Saar BG, Friedrich MG, Chen F, Liu Y-S, Dixon RA, Himmel ME, Xie XS, Ding S-Y (2010) Imaging Lignin-Downregulated Alfalfa Using Coherent Anti-Stokes Raman Scattering Microscopy. Bioenerg. Res. 3(3): 272-277.

[166] Larsen KL, Barsberg S (2010) Theoretical and Raman spectroscopic studies of phenolic lignin model monomers. J. Phys. Chem. B 114(23): 8009-8021.

[167] Agarwal UP (2006) Raman imaging to investigate ultrastructure and composition of plant cell walls: distribution of lignin and cellulose in black spruce wood (*Picea mariana*). Planta 224(5): 1141-1153.

[168] Gierlinger N, Schwanninger M (2007) The potential of Raman microscopy and Raman imaging in plant research - review. Spectroscopy 21: 69-89.

[169] Agarwal UP, Ralph SA (2008) Determination of ethylenic residues in wood and TMP of spruce by FT-Raman spectroscopy. Holzforschung 62(6): 667-675.

[170] Hanninen T, Kontturi E, Vuorinen T (2011) Distribution of lignin and its coniferyl alcohol and coniferyl aldehyde groups in *Picea abies* and *Pinus sylvestris* as observed by Raman imaging. Phytochemistry 72(14-15): 1889-1895.

[171] Carpita NC, Gibeaut DM (1993) Structural models of primary cell walls in flowering plants: consistency of molecular structure with the physical properties of the walls during growth. Plant J. 3(1): 1-30.

[172] Carpita NC, McCann MC (2000) The cell wall. In: Buchanan BB GW, Jones RL, editor. American Society of Plant Biologists; Rockville, MD: Biochemistry and Molecular Biology of Plants.

[173] Carpita NC (1996) Structure and biogenesis of the cell walls of grasses. Annu. Rev. Plant Physiol. Plant Mol. Biol. 47: 445-476.

[174] Scalbert A, Monties B, Lallemand J-Y, Guittet E, Rolando C (1985) Ether linkage between phenolic acids and lignin fractions from wheat straw. Phytochemistry 24(6): 1359-1362.

[175] Piot O, Autran J-C, Manfait M (2001) Investigation by confocal Raman microspectroscopy of the molecular factors responsible for grain cohesion in the *Triticum aestivum* bread wheat. Role of the cell walls in the starchy endosperm. J. Cereal Sci. 34(2): 191-205.

[176] Ram MS, Dowell FE, Seitz LM (2003) FT-Raman spectra of unsoaked and NaOH-soaked wheat kernels, bran, and ferulic acid. Cereal Chem. 80(2): 188-192.

[177] Sun L, Simmons BA, Singh S (2011) Understanding tissue specific compositions of bioenergy feedstocks through hyperspectral Raman imaging. Biotechnol. Bioeng. 108(2): 286-295.

[178] Agarwal UP (1999) Chapter 9: An Overview of Raman Spectroscopy as Applied to Lignocellulosic Materials. In: Argyropoulos DS, editor. Advances in Lignocellulosics Characterization. Atlanta: TAPPI PRESS; p. 201-225.

[179] Agarwal UP, McSweeny JD, Ralph SA (2011) FT-Raman investigation of milled-wood lignins: Softwood, hardwood, and chemically modified black spruce lignins. J. Wood Chem. Technol. 31(4): 324-344.

[180] Sebastian S, Sundaraganesan N, Manoharan S (2009) Molecular structure, spectroscopic studies and first-order molecular hyperpolarizabilities of ferulic acid by density functional study. Spectroc. Acta Pt. A-Molec. Biomolec. Spectr. 74(2): 312-323.

[181] Atalla RH, Agarwal UP, Bond JS (1992) Raman Spectroscopy. In: Lin SY, Dence CW, editors. Methods in Lignin Chemistry. Heidelberg, Germany: Springer-Verlag; p. 162-176.

[182] Pu YQ, Kosa M, Kalluri UC, Tuskan GA, Ragauskas AJ (2011) Challenges of the utilization of wood polymers: how can they be overcome? Appl. Microbiol. Biotechnol. 91(6): 1525-1536.

[183] Gierlinger N, Schwanninger M (2006) Chemical imaging of poplar wood cell walls by confocal Raman microscopy. Plant Physiol. 140(4): 1246-1254.

[184] Takayama M, Johjima T, Yamanaka T, Wariishi H, Tanaka H (1997) Fourier transform Raman assignment of guaiacyl and syringyl marker bands for lignin determination. Spectroc. Acta Pt. A-Molec. Biomolec. Spectr. 53: 1621-1628.

[185] Larsen KL, Barsberg S (2011) Environmental Effects on the Lignin Model Monomer, Vanillyl Alcohol, Studied by Raman Spectroscopy. J. Phys. Chem. B 115(39): 11470-11480.

[186] Schmidt M, Schwartzberg AM, Perera PN, Weber-Bargioni A, Carroll A, Sarkar P, Bosneaga E, Urban JJ, Song J, Balakshin MY, Capanema EA, Auer M, Adams PD, Chiang VL, Schuck PJ (2009) Label-free in situ imaging of lignification in the cell wall of low lignin transgenic *Populus trichocarpa*. Planta 230(3): 589-597.

[187] Horvath L, Peszlen I, Gierlinger N, Peralta P, Steve K, Csoka L (2012) Distribution of wood polymers within the cell wall of transgenic aspen imaged by Raman microscopy. Holzforschung DOI 10.1515/hf-2011-0126.

[188] Jacobs BF, Kingston JD, Jacobs LL (1999) The origin of grass-dominated ecosystems. Annals of the Missouri Botanical Garden: Missouri Botanical Garden Press; p. 590-643.

[189] Draper J, Mur LAJ, Jenkins G, Ghosh-Biswas GC, Bablak P, Hasterok R, Routledge APM (2001) Brachypodium distachyon. A New Model System for Functional Genomics in Grasses. Plant Physiol. 127(4): 1539-1555.

[190] Albert L, Németh ZI, Halász G, Koloszár J, Varga S, Takács L (1999) Radial variation of pH and buffer capacity in the red-heartwooded beech (*Fagus silvatica* L.) wood. Holz als Roh- und Werkst. 57: 75-76.

[191] Somerville C, Bauer S, Brininstool G, Facette M, Hamann T, Milne J, Osborne E, Alex P, Persson S, Raab T, Vorwerk S, Youngs H (2004) Toward a systems approach to understanding plant cell walls. Science 206: 2206-2211.

[192] Grabber JH, Ralph J, Lapierre C, Barriere Y (2004) Genetic and molecular basis of grass cell-wall degradability. I. Lignin-cell wall matrix interactions. C. R. Biol. 327(5): 455-465.

[193] Ralph J, Grabber JH, Hatfield RD (1995) Lignin-ferulate cross-links in grasses: active incorporation of ferulate polysaccharide esters into ryegrass lignins. Carbohydr. Res. 275(1): 167-178.

[194] Ralph J, Hatfield RD, Sederoff RR, MacKay JJ (1998) Order and randomness in lignin and lignification: Is a new paradigm for lignification required? Research Summaries: 39-41.